NUREG/CR-5237
LA-11444-MS

Use of Linear Reduced–Stiffness Analytical Models to Predict Seismic Response of Damaged Concrete Structures

Prepared by C. R. Farrar, C. M. Alvord

Los Alamos National Laboratory

Prepared for
U.S. Nuclear Regulatory Commission

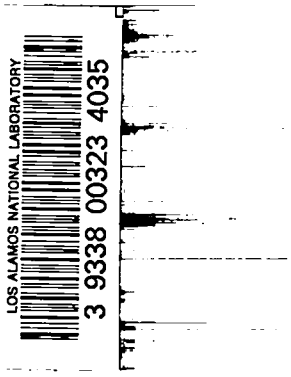

AVAILABILITY NOTICE

Availability of Reference Materials Cited in NRC Publications

Most documents cited in NRC publications will be available from one of the following sources:

1. The NRC Public Document Room, 2120 L Street, NW, Lower Level, Washington, DC 20555

2. The Superintendent of Documents, U.S. Government Printing Office, P.O. Box 37082, Washington, DC 20013-7082

3. The National Technical Information Service, Springfield, VA 22161

Although the listing that follows represents the majority of documents cited in NRC publications, it is not intended to be exhaustive.

Referenced documents available for inspection and copying for a fee from the NRC Public Document Room include NRC correspondence and internal NRC memoranda; NRC Office of Inspection and Enforcement bulletins, circulars, information notices, inspection and investigation notices; Licensee Event Reports; vendor reports and correspondence; Commission papers; and applicant and licensee documents and correspondence.

The following documents in the NUREG series are available for purchase from the GPO Sales Program: formal NRC staff and contractor reports, NRC-sponsored conference proceedings, and NRC booklets and brochures. Also available are Regulatory Guides, NRC regulations in the *Code of Federal Regulations*, and *Nuclear Regulatory Commission Issuances*.

Documents available from the National Technical Information Service include NUREG series reports and technical reports prepared by other federal agencies and reports prepared by the Atomic Energy Commission, forerunner agency to the Nuclear Regulatory Commission.

Documents available from public and special technical libraries include all open literature items, such as books, journal and periodical articles, and transactions. *Federal Register* notices, federal and state legislation, and congressional reports can usually be obtained from these libraries.

Documents such as theses, dissertations, foreign reports and translations, and non-NRC conference proceedings are available for purchase from the organization sponsoring the publication cited.

Single copies of NRC draft reports are available free, to the extent of supply, upon written request to the Office of Information Resources Management, Distribution Section, U.S. Nuclear Regulatory Commission, Washington, DC 20555.

Copies of industry codes and standards used in a substantive manner in the NRC regulatory process are maintained at the NRC Library, 7920 Norfolk Avenue, Bethesda, Maryland, and are available there for reference use by the public. Codes and standards are usually copyrighted and may be purchased from the originating organization or, if they are American National Standards, from the American National Standards Institute, 1430 Broadway, New York, NY 10018.

DISCLAIMER NOTICE

NUREG/CR-5237
LA-11444-MS
RD

Use of Linear Reduced-Stiffness Analytical Models to Predict Seismic Response of Damaged Concrete Structures

Manuscript Completed: September 1988
Date Published: May 1989

Prepared by
C. R. Farrar, C. M. Alvord

Los Alamos National Laboratory
P.O. Box 1663
Los Alamos, NM 87545

Prepared for
Division of Engineering
Office of Nuclear Regulatory Research
U.S. Nuclear Regulatory Commission
Washington, DC 20555
NRC FIN A7221

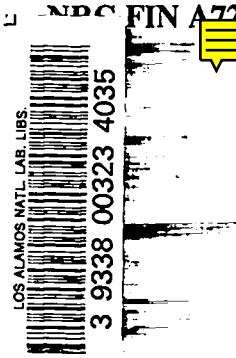

CONTENTS

FIGURES

TABLES

USE OF LINEAR REDUCED-STIFFNESS ANALYTICAL MODELS TO PREDICT SEISMIC RESPONSE OF DAMAGED CONCRETE STRUCTURES

by

Charles R. Farrar and Christina M. Alvord

ABSTRACT

An extensive analysis of previously measured seismic response data from the Seismic Category I Structures program was made to determine if reduced stiffness linear models can be used to predict the response of damaged nuclear power plant structures. Four structures ranging from one to three stories were analyzed for three different peak acceleration inputs. All inputs were scaled versions of the 1940 El Centro earthquake measured at the base of the test structures during shake-table testing. Comparisons between measured and analytically predicted responses were made in terms of floor response spectra. Stiffness in the analytical models was adjusted to obtain a match in frequency and damping was adjusted to obtain a match in amplitude. Results showed that the reduced-stiffness linear models could accurately predict the response of the damaged structures and these results were consistent with the response observed during static cyclic testing of similar structures. Changes in damping with excitation levels are also discussed. In addition to the analysis of the seismic response data, the stiffness of these structures was analyzed by a variety of methods currently used by industry and the stiffness values were compared with the values in the analytical models that best fit the measured response.

I. INTRODUCTION

The Seismic Category I Structures Program is being carried out at the Los Alamos National Laboratory under sponsorship of the U.S. Nuclear Regulatory Commission (NRC), Office of Nuclear Regulatory Research. The program has the objective of investigating the structural dynamic response of Seismic Category I reinforced concrete structures (exclusive of containment) that are subjected

to seismic loads beyond their design basis. The program, as originally conceived, is a combined experimental/analytical investigation with heavy emphasis on the experiment component to establish a good data base. A number of meetings and interactions with the NRC staff have led to the following set of specific program objectives:

1. Address the seismic response of reinforced concrete Category I structures, other than containments.
2. Develop experimental data for determining the sensitivity of structural behavior of Category I structures in the elastic and inelastic response range to variations in configuration, design practices, and earthquake loading.
3. Develop experimental data to enable validation of computer programs used to predict the behavior of Category I structures during earthquake motions that cause elastic and inelastic responses.
4. Identify floor response spectra changes that occur during earthquake motions that cause elastic and inelastic structural responses.
5 Develop a method for representing damping in the inelastic range and demonstrate how this damping changes when structural response goes from the elastic to the inelastic ranges.
6. Assess how shifts in structural frequency affect plant risk.

To meet these objectives, personnel at Los Alamos have tested, statically and/or dynamically, small-scale isolated shear walls, diesel generator building models, auxiliary building models and large-scale shear wall elements. A more detailed summary of the motivation for these tests, scale model theory, model construction, testing procedures and test results can be found in Refs. 1-8.

This document reports the analytical work carried out in FY 87 as part of an effort to address program objectives 4 and 5. Specifically, at the Technical Review Group* (TRG) meeting on December 19, 1986, the TRG requested that the investigators at Los Alamos attempt to match floor response spectra

---

* The Technical Review Group is a group of nationally recognized seismic and concrete experts on nuclear power plant structures and was established to both review the progress and make recommendations regarding the technical direction of this program.

calculated from acceleration-time histories measured on different structures previously tested as part of the program (herein referred to as measured response spectra) with floor response spectra determined from the response of analytical models of the same structures (herein referred to as calculated response spectra). The calculated response spectra were to be generated from the response of linear analytical models of the test structures subjected to actual measured base inputs. Matching was to be accomplished by adjusting the stiffness and damping in the analytical model. The motivation of this investigation was based on TRG's feeling that more emphasis should be placed on the analysis of data already obtained in the program. In particular, the TRG felt that it was pertinent to determine if the Seismic Category I structures can continue to be analyzed with corrected linear models despite the reductions in stiffness associated with the seismic loading. Also, comparisons between measured and analytical response spectra quantify the differences between the predicted response of these structures based on current design practices and the experimentally observed response as this information would actually be used by the engineer in plant and equipment design.

The TRG also requested that engineers at Los Alamos use various design assumptions to recompute the analytical values of stiffners for several, different test structure geometries. These alternate values of stiffness were then to be compared with the indirectly measured stiffness values as inferred from resonant frequency measurements.

II. RESPONSE SPECTRA CALCULATIONS

Attempts to predict the measured response spectra with calculated response spectra were performed on four structures. These structures included a small-scale shear wall element (Ref. 6), a large-scale shear wall element (Ref. 7), a two-story, 1/10-scale diesel generator building model (Ref. 3), and a three-story, 1/42-scale auxiliary building model (Ref. 5). The structures that were analyzed are shown in Figs. 1-4, respectively, and their material properties are summarized in Table I. For each structure, three different peak acceleration level base excitations were analyzed. These excitations were scaled versions of the 1940 El Centro earthquake. With the different levels of excitation, insight can be gained into the change in structural properties (damping and stiffness) as a function of the seismic input amplitude. By analyzing

TABLE I

TEST STRUCTURES MATERIAL PROPERTIES

Structure	Ultimate Compressive Strength (Ksi)	Modulus of Elasticity (psi)	$57{,}000\sqrt{f'_c}$ (psi)	Reinforcement %, each direction
Small-scale shear wall element, TRG-1	3.77	3.2×10^6	3.5×10^6	0.56
Large-scale shear wall element, TRG-3	3.81	2.0×10^6	3.5×10^6	0.61
1/30-scale diesel generator building, CERL-1	3.18	2.8×10^6	3.2×10^6	0.56
1/42-scale auxiliary building, SANDIA-1	2.90	2.7×10^6	3.1×10^6	0.56

responses to different excitation amplitudes one can also determine if the test structures are behaving in a linear manner.

The numerical models that were used to determine the analytical response spectra were discrete lumped mass models typical of those used by the nuclear civil engineering community (Ref. 9). Only translational degrees of freedom were associated with each floor level. A fourth-order Runge-Kutta computation procedure was used to integrate the equations of motion developed from the numerical model. Initial estimates of stiffness were determined indirectly from the measured first-mode resonant frequency assuming the following relationship:

$$\left(\frac{f_m}{f_T}\right)^2 = \sqrt{\frac{K_i}{K_T}} \quad ,$$

where f_m = the measured first mode resonant frequency.

f_T = the theoretical first mode resonant frequency.

K_T = theoretical stiffness (based on uncracked cross-section, strength-of-materials analysis).

K_i = initial estimate of the stiffness to be used in the numerical lumped mass models.

Figure 5 shows the ratio of the initial stiffness estimate to the theoretical stiffness for the test structures that were analyzed. Damping was initially estimated at 7% of critical, based on damping ratios identified from frequency response functions measured during previous testing in the program. In this report all damping values refer to viscous damping, percent of critical. The empirical methods used to lump mass at a particular floor level are discussed in the summary of the response spectra analyses for the individual test structures.

To find the structural properties for an analytical model whose response would simulate the measured floor response spectra, an iterative process was pursued during which stiffness was adjusted to match the frequency of the measured peak response and damping was adjusted to match the amplitude of the measured peak response. Visual inspection of the response spectra was used to determine if the analytical model predicted the measured response. A sum-of-the-errors squared analysis could have been used to quantify the match between measured and analytical response spectra. However, it was felt that a stray high-frequency spike in the measured floor response spectra could lead to a poor numerical value for the fit even though the strong-motion portion of the response was well predicted. The following steps outline the iterative procedure used to match the measured and analytical floor response spectra.

1. Digitize all necessary analog accelerometer signals, apply the appropriate calibration factors, filter 60-Hz noise and baseline correct for dc offset.
2. Calculate the measured floor response spectra using the digitized signals from step 1 and using 2% equipment damping.
3. Develop a lumped-mass analytical model of the test structure and subject it to the measured base input (digitized in step 1).

4. Calculate floor response spectra based on the response of the analytical model as determined in step 3. Use 2% equipment damping.
5. Repeat steps 3 and 4 adjusting stiffness in the model to match measured response spectra peaks in terms of frequency (often requiring several iterations).
6. Repeat steps 3 and 4 adjusting damping in the model to match the amplitude of the peaks in the measured response spectra (often requiring several iterations).
7. Repeat steps 2-6 for 10% equipment damping.

III. RESULTS OF RESPONSE SPECTRA MATCHING

A summary of the response spectra analyses for each test structure follows. No scaling of the results was made. If an individual would like to scale the results to a prototype structure, Ref. 4 and the report discussing the particular test structure should be consulted. In the discussion that follows, the theoretical stiffness refers to the uncracked cross-section, strength-of-materials stiffness using a measured modulus of elasticity and assuming the entire end walls were effective in resisting bending deformations. Included on all plots comparing the measured response spectra (labeled measured) and the best estimate analytical response spectra (labeled analytical with reduced stiffness) is a plot of analytical response spectra using the theoretical stiffness (labeled analytical, a current design practice). All the response spectra have been displayed in terms of absolute accelerations and 2% damping was used to calculate the base input response spectra.

A. Response Spectra Analysis of TRG-1

The structure shown in Fig. 1 is referred to as TRG-1. This structure was analyzed for response to 0.211-g's, 2.54-g's, and 7.23-g's peak acceleration simulated seismic inputs. The response spectra for these base excitations are shown in Figs. 6-8. Figure 5 shows the measured stiffness in TRG-1 to be 38% of the theoretical value. This stiffness reduction was applied to the theoretical stiffness in a one degree-of-freedom, lumped-mass, analytical model that had 7% damping. The lumped mass was taken as the added mass, the mass of the top slab plus the mass of one slab thickness of the walls. Figures 9 and 10 show the comparison between the measured response spectra and the calculated

response spectra for the 0.211-g's input. As is evident from these figures, the strong motion portion of the measured response was predicted by the analytical model.

During the subsequent analyses of the response to the two higher-level inputs, the stiffness in the analytical model had to be reduced and the damping in these models had to be increased in order to accurately predict the measured response. The response spectra corresponding to the 2.54-g's input are shown in Figs. 11 and 12 and the response spectra for the 7.23-g's input are shown in Figs. 13 and 14. Changes in the structural properties that were necessary to obtain agreement with the measured response spectra are indicative of the damage that the structure experienced during the testing sequence. These properties are summarized in Table II.

TABLE II

STRUCTURAL PROPERTIES USED IN THE BEST-FIT ANALYTICAL MODEL OF TRG-1

Excitation Level	Lumped Mass ($lb\text{-}s^2/in.$)	Stiffness ($lb/in. \times 10^{-6}$)	Damping* (% of critical)
0.211 g's	1.65	0.44	7 7
2.54 g's	1.65	0.31	22 22
7.23 g's	1.65	0.15	16 13

*For a particular input level, the first damping value corresponds to the best fit for 2% equipment damping FRS and the second damping value corresponds to the best fit for 10% equipment damping FRS.

B. Response Spectra Analysis of TRG-3

The structure shown in Fig. 2 is referred to as TRG-3. This structure was analyzed for response to 0.88-g's, 0.99-g's, and 1.65-g's peak acceleration simulated seismic inputs. The response spectra for these base excitations are shown in Figs. 15-17.

As revealed by Fig. 5, the measured stiffness appeared to be 25% of the theoretical stiffness. Initially, this stiffness reduction was applied to the

theoretical stiffness in a one degree-of-freedom lumped-mass analytical model that had 7% damping. A stiffness value that was 17% of the theoretical stiffness was found to provide the best match to the measured response. The difference between this stiffness value and the one determined from the measured resonant frequency is attributed to the nonlinear response of the structure. The reduction in stiffness to 25% of the theoretical stiffness was determined from the response to a low-level (less than 0.5-g's peak acceleration) haversine pulse after the structure had been damaged seismically. When excited by the 0.88-g's seismic input, the change in frequency content and amplitude of the excitation produced a different response in the damaged structure. The lumped mass for the analytical model of this structure was determined in a similar fashion as the lumped mass for TRG-1. A damping value of 8.5% was needed to match the measured response spectra when they were calculated with 2% equipment damping. When 10% equipment damping was used, the analytical model required only 5.5% damping to obtain an accurate match. The same analytical model was used with all three seismic inputs and found to work equally well at all levels. This implies that the structure was responding in a reduced-stiffness, linear manner and that the subsequent seismic excitations did not introduce further damage. The comparisons of response spectras for the 0.88-g's input are shown in Figs. 18 and 19. For the 0.99-g's input, the comparisons are shown in Figs. 20 and 21, and for the 1.65-g's input, the comparisons are shown in Figs. 22 and 23. TRG-3 was the only structure made with conventional concrete and rebar that was studied in this exercise.

C. Response Spectra Analysis of the 1/10-Scale Diesel Generator Building Model

The structure shown in Fig. 3 is a 1/10-scale model of an idealized diesel generator building and is referred to as CERL-1. This structure was analyzed for response to 1.88-g's, 3.53-g's, and 13.66-g's peak acceleration simulated seismic inputs. The 13.6-g's input was the final seismic test this structure experienced before failure. Response spectra for these base excitations are shown in Figs. 24-26. Figure 27 shows the lumped-mass model used to calculate the analytical responses of the CERL-1 structure.

During a particular seismic excitation, the same stiffness values were used for each floor. Again, the lumped masses were taken as the added mass plus the floor slab mass plus the mass of one slab thickness of the walls above and below the floor.

Initially, for the 1.88-g's input, the stiffness was reduced to 17% of the theoretical stiffness to match the measured response. Damping values of 6% for each floor provided the best match to the measured response. Comparisons of the measured and analytically predicted FRS are shown in Figs. 28-31 for the 1.88-g's excitation. As the peak input acceleration was increased, the stiffness values were decreased and the damping values were increased to obtain a match with the measured spectra. For both the 3.53-g's and the 13.6-g's excitations, damping in the bottom floor of the analytical model had to be made greater than the damping associated with the top floor to obtain a match to the measured data. Comparisons of the measured and analytically predicted FRS are shown in Figs. 32-35 for the 3.53-g's input and similar comparisons are shown in Figs. 36-39 for the 13.66-g's input. The structural properties that provided the best estimate to the measured response are summarized in Table III.

TABLE III

STRUCTURAL PROPERTIES USED IN THE BEST-FIT ANALYTICAL MODEL OF CERL-1 (Fig. 27)

Excitation Level	Lumped Mass ($lb\text{-}s^2/in.$)	Stiffness ($lb/in. \times 10^{-6}$)	Damping (% of critical)
1.88 g's	$m_1 = 4.69$ $m_2 = 4.61$	$K_1 = 1.4$ $K_2 = 1.4$	$\zeta_1 = 6$ $\zeta_2 = 6$
3.53 g's	$m_1 = 4.69$ $m_2 = 4.61$	$K_1 = 1.4$ $K_2 = 1.4$	$\zeta_1 = 15$ $\zeta_2 = 11$
13.6 g's	$m_1 = 4.69$ $m_2 = 4.61$	$K_1 = 0.65$ $K_2 = 0.65$	$\zeta_1 = 35$ $\zeta_2 = 10$

D. Response Spectra Analysis of the 1/42-Scale Auxiliary Building Model

The structure shown in Fig. 4 is a 1/42-scale model of an idealized auxiliary building and is referred to as SANDIA-1. This structure was analyzed for response to 0.65-g's, 1.27-g's, and 2.83-g's peak acceleration simulated seismic inputs. Response spectra for these base excitations are shown in Figs. 40-42. Figure 43 shows the lumped mass model used to calculate the analytical responses of the SANDIA-1 structure.

For all three levels of excitation, a reduction to 25% of the theoretical stiffness in the analytical model was found to give the best correspondence between the measured and the computed response. Similar trends were seen with the damping as had been noted with the CERL-1 structure. That is, to obtain a good match, damping was increased in the lower stories with the value used in the bottom story playing the most significant role in the overall structural response. Comparisons of the measured and analytically predicted FRS are shown in Figs. 44-49 for the 0.65-g's excitation.

For the 1.27-g's input, three sets of damping values were used to obtain "best estimates" of the measured response. The first set, ζ_1 = 9%, ζ_2 = 4%, and ζ_3 = 2%, matched the top floor response best but significantly overestimated the bottom floor response. Because the top floor sees the largest response, this estimate may be said to be the best. The second set, ζ_1 = 11%, ζ_2 = 6%, and ζ_3 = 2%, matched the bottom floor response but significantly underestimated the top floor response. Finally, the third set ζ_1 = 8%, ζ_2 = 7%, and ζ_3 = 6%, provided the best overall estimate but still slightly overestimated the bottom floor response and slightly underestimated the top floor response while giving a very accurate estimate of the second floor response. Comparisons of these measured and analytically predicted FRS are shown in Figs. 50-55 and similar plots for the 1.27-g's input but with stiffnesses determined by different design assumptions are shown in Figs. 56-61. Figures 62-67 show the response spectra matching for the 2.83-g's input. The structural properties that provided the best estimate to the measured response are summarized in Table IV.

IV. ALTERNATE STIFFNESS CALCULATIONS

In addition to calculating linear "best estimate" response spectra that match the measured response spectra, several design assumptions have been used to calculate alternate values of the shear wall stiffness. Among the assumptions are the following: the end walls are fully effective in resisting bending deformations, the end wall provides no resistance, ACI 349-85 T-beam criteria are used for assessing the end wall's effectiveness, and the ASCE 4-86 method is used for assessing the end wall's effectiveness. These stiffness values have been calculated with both the measured modulus of elasticity and with a modulus calculated from the ACI 349-85 empirical formula. In Table V, the

TABLE IV

STRUCTURAL PROPERTIES USED IN THE BEST-FIT ANALYTICAL MODEL OF SANDIA-1

(Fig. 43)

Excitation Level	Lumped Mass ($lb\text{-}s^2/in.$)	Stiffness ($lb/in. \times 10^{-6}$)	Damping (% of critical)
0.65 g's	$m_1 = 1.48$ $m_2 = 1.37$ $m_3 = 1.18$	$K_1 = 1.37$ $K_2 = 1.37$ $K_3 = 1.37$	$\zeta_1 = 12$ $\zeta_2 = 7$ $\zeta_3 = 4$
1.27 g's	$m_1 = 1.48$ $m_2 = 1.37$ $m_3 = 1.18$	$K_1 = 1.37$ $K_2 = 1.37$ $K_3 = 1.37$	$\zeta_1 = 8$ $\zeta_2 = 7$ $\zeta_3 = 6$
2.83g's	$m_1 = 1.48$ $m_2 = 1.37$ $m_3 = 1.18$	$K_1 = 1.37$ $K_2 = 1.37$ $K_3 = 1.37$	$\zeta_1 = 15$ $\zeta_2 = 14$ $\zeta_3 = 13$

stiffness values are compared to the ones that provided the best match between the analytical and measured response spectra at the lowest simulated seismic input level. In all cases, the reinforcing steel has been neglected in the computation of the cross-sectional moment of inertia and effective shear area.* For the CERL-1 and SANDIA-1 structures, the stiffness values are for an individual story assuming cantilever deformation. Parameters for these calculations are summarized in Table V. All calculations assume Poisson's ratio (ν) equals 0.2. The structures' geometries are shown in Figs. 1-4 and 68. Figure 68 shows a structure (TRG-4) that was tested statically.

A. Stiffness Parameters for TRG-1

$$\frac{1}{K_T} = \frac{1}{K_{BM}} + \frac{1}{K_{CB}} + \frac{1}{K_S} \quad ,$$

$$K_{BM} = \frac{2E_c I}{hL^2} \quad , \qquad \text{Bending stiffness associated with applied moment}$$

* TRG-3 had the largest percentage of reinforcement and smallest concrete modulus. Including the reinforcement in the stiffness calculation increased the stiffness value by 12%.

TABLE V

ANALYTICAL STIFFNESS VALUES COMPARED WITH MEASURED STIFFNESS VALUES

	Stiffness Determined from Seismic Response [e]	Stiffness Determined from Response Spectra Matching	End Walls Fully Effective	ASCE Criteria	ACI T-Beam Criteria	Neglect End Walls
	lb/in. x 10^{-6}	lb/in. x 10^{-6}		lb/in. x 10^{-6}		
TRG-1 (1 story)[a]	0.41	0.44	1.07	0.93	0.61	0.44
TRG-1 (1 story)[b]	0.41	0.44	1.17	1.02	0.66	0.48
TRG-3 (1 story)[a]	0.67	0.45	2.67	2.33	1.54	1.11
TRG-3 (1 story)[b]	0.67	0.45	4.67	4.07	2.70	1.94
CERL-1 (2 story)[a,d]	1.31	1.4	8.21	6.88	2.00	1.94
CERL-1 (2 story)[b,d]	1.31	1.4	9.38	7.86	2.29	2.22
Sandia (3 story)[a,d]	1.39	1.37	5.45	5.11	4.82	4.68
Sandia (3 story)[b,d]	1.39	1.37	6.26	5.86	5.53	5.37
TRG-4 (1 story)[a]	6.49[c]	--	6.27	5.39	3.88	2.51
TRG-4 (1 story)[b]	6.49[c]	--	7.14	6.15	4.42	2.86

---

a Theoretical values calculated using measured modulus of elasticity

b Theoretical values calculated using $E_c = 57{,}000 \sqrt{f'_c}$

c These stiffness values were determined from static load cycle testing using external displacement gages

d These stiffness values are for an individual story assuming cantilever deformation

e These stiffness values were determined from

$$K = \left\{ \frac{f_{meas.}}{f_{Theory}} \right\}^2 K_{Theory} .$$

$$K_{CB} = \frac{3E_c I}{L^3} \quad , \quad \text{Bending stiffness associated with applied load}$$

$$K_S = \frac{AG}{L} \quad , \quad \text{Shear stiffness}$$

$$A = 22.5 \text{ in.} \times 1 \text{ in.} = 22.5 \text{ in.}^2$$

$$E_c = \begin{cases} 3.2 \times 10^6 \text{ psi (measured)} \\ 3.5 \times 10^6 \text{ psi (ACI)} \end{cases}$$

$$G = \frac{E_c}{2(1+\nu)} = \begin{cases} 1.33 \times 10^6 & \text{(measured)} \\ 1.46 \times 10^6 & \text{(ACI)} \end{cases}$$

$L = 22.5$ in. (See free-body diagram, Fig. 69)

$h = 3.125$ in. (See free-body diagram, Fig. 69)

$$I = \frac{1}{12} 30 (22.5^3) - 2 \frac{1}{12} 14.5 (20.5)^3 = 7700 \text{ in.}^4 \quad ,$$

$$I_{\substack{\text{ACI T-beam} \\ \text{ACI 349-85, 8.10.4} \\ \text{(Fig. 70)}}} = \frac{1}{12} 4(22.5)^3 - 2 \left[\frac{1}{12} 1.5 (20.5)^3 \right] = 1600 \text{ in.}^4 \quad ,$$

$$I_{\substack{\text{neglect end} \\ \text{walls}}} = \frac{1}{12} 1(22.5)^3 = 950 \text{ in.}^4 \quad .$$

$$I_{\text{ASCE 4-86}} = \frac{1}{12} 16 (22.5)^3 - 2 \left[\frac{1}{12} 7.5 (20.5)^3 \right] = 4400 \text{ in.}^4$$

(Fig. 71)

B. Stiffness Parameters for TRG-3

$$\frac{1}{K_T} = \frac{1}{K_{BM}} + \frac{1}{K_{CB}} + \frac{1}{K_s} \quad ,$$

$$K_{BM} = \frac{2E_c I}{hL^2} \quad ,$$

$$K_{CB} = \frac{3E_c I}{L^3} \quad ,$$

$$K_s = \frac{AG}{L} \quad ,$$

$$A = 90 \times 4 = 360 \text{ in.}^2$$

$$E_c = \begin{cases} 2.0 \times 10^6 \text{ psi (measured)} \\ 3.5 \times 10^6 \text{ psi (ACI)} \end{cases} \quad ,$$

$$G = \frac{E_c}{2(1+\nu)} = \begin{cases} 8.33 \times 10^5 \text{ psi (measured)} \\ 1.46 \times 10^6 \text{ psi (ACI)} \end{cases} \quad ,$$

$L = 90$ in. (See free-body diagram, Fig. 69)

$h = 12.5$ in. (See free-body diagram, Fig. 69)

$$I = \frac{1}{12} 120(90)^3 - 2\left[\frac{1}{12} 58(82)^3\right] = 1{,}960{,}000 \text{ in.}^4,$$

$$I_{\substack{\text{ACI T-beam} \\ \text{ACI 349-85, 8.10.4}}} = \frac{1}{12} 16(90)^3 - 2\left[\frac{1}{12} 6(82)^3\right] = 421{,}000 \text{ in.}^4 \quad ,$$

$$I_{\substack{\text{neglect end} \\ \text{walls}}} = \frac{1}{12} 4(90)^3 = 243{,}000 \text{ in.}^4 \quad .$$

$$I_{\text{ASCE 4-86}} = \frac{1}{12} 64\,(90)^3 - 2\left[\frac{1}{12} 30\,(82)^3\right] = 1{,}130{,}000 \text{ in.}^4 \quad .$$

C. Stiffness Parameters for CERL-1

$$\frac{1}{K_T} = \frac{1}{K_{CB}} + \frac{1}{K_s} \quad ,$$

$$\frac{1}{K_{CB}} = \frac{3E_c I}{L^3} \quad ,$$

$$\frac{1}{K_s} = \frac{AG}{L} \quad ,$$

$$A = 2(3 \times 30) = 180 \text{ in.}^2$$

$$E_c = \begin{cases} 2.8 \times 10^6 \text{ psi (measured)} \\ 3.2 \times 10^6 \text{ psi (ACI)} \end{cases},$$

$$G = \frac{E_c}{2(1+\nu)} = \begin{cases} 1.17 \times 10^6 \text{ psi (measured)} \\ 1.38 \times 10^6 \text{ psi (ACI)} \end{cases},$$

$$L = 21.75 \text{ in.}$$

$$I = \frac{1}{12} 54(30)^3 - 2\left[\frac{1}{12} 48(24)^3\right] = 66{,}000 \text{ in.}^4 ,$$

$$I_{\substack{\text{ACI T-beam} \\ \text{ACI 349-85, 8.10.3}}} = 2\left[\frac{1}{12} 4.8(30)^3\right] - 2\left[\frac{1}{12} 1.8\ (24)^3\right] = 17{,}000 \text{ in.}^4$$

(Fig. 72)

$$I_{\substack{\text{neglect} \\ \text{end walls}}} = 2\left[\frac{1}{12} 3(30)^3\right] = 14{,}000 \text{ in.}^4 .$$

$$I_{\text{ASCE 4-86}} = 2\left[\frac{1}{12} 10.25\ (30)^3\right] - 2\left[\frac{1}{12} 7.25\ (24)^3\right] = 29{,}000 \text{ in.}^4 .$$

(Fig. 73)

D. Stiffness Parameters for the Sandia Structure

$$\frac{1}{K_T} = \frac{1}{K_{CB}} + \frac{1}{K_s} ,$$

$$\frac{1}{K_{CB}} = \frac{3E_c I}{L^3} ,$$

$$\frac{1}{K_s} = \frac{AG}{L} ,$$

$$A = 2[1 \times 26] = 52 \text{ in.}^2 ,$$

$$E_c = \begin{cases} 2.7 \times 10^6 \text{ psi (measured)} \\ 3.1 \times 10^6 \text{ psi (ACI)} \end{cases},$$

$$G = \frac{E_c}{2(1+\nu)} = \begin{cases} 1.12 \times 10^6 \text{ psi (measured)} \\ 1.29 \times 10^6 \text{ psi (ACI)} \end{cases}$$

$L = 10$ in.,

$$I = \frac{1}{12} 26(26)^3 - 2\left[\frac{1}{12} 24(24)^3\right] = \text{ in.}^4 = 10{,}500 \text{ in.}^4$$

$$I_{\substack{\text{ACI T-beam} \\ \text{ACI 349-85, 8.10.3}}} = 2\left[\frac{1}{12} 1.83(26)^3\right] - 2\left[\frac{1}{12} 0.83(24)^3\right] = 3450 \text{ in.}^4 ,$$

$$I_{\substack{\text{neglect} \\ \text{end walls}}} = 2\left[\frac{1}{12} 1(26)^3\right] = 2930 \text{ in.}^4 ,$$

$$I_{\text{ASCE 4-86}} = 2\left[\frac{1}{12} 4.33\ (26)^3\right] - 2\left[\frac{1}{12} 3.33\ (24)^3\right] = 5010 \text{ in.}^4$$

E. Stiffness Parameters for TRG-4

$$\frac{1}{K_T} = \frac{1}{K_{BM}} + \frac{1}{K_{CB}} + \frac{1}{K_S} ,$$

$$K_{BM} = \frac{2E_c I}{hL^2} ,$$

$$K_{CB} = \frac{3E_c I}{L^3} .$$

$$K_S = \frac{AG}{L} ,$$

$A = 90 \times 6 = 540 \text{ in.}^2$

$$E = \begin{cases} 3.23 \times 10^6 \text{ psi (measured)} \\ 3.68 \times 10^6 \text{ psi (ACI)} \end{cases}$$

$$G = \frac{E_c}{2(1+\nu)} = \begin{cases} 1.35 \times 10^6 \text{ psi (measured)} \\ 1.53 \times 10^6 \text{ psi (ACI)} \end{cases},$$

$h = 20$ in.,

$L = 90$ in.,

$$I = \frac{1}{12} 120(90)^3 - 2\left[\frac{1}{12} 57(78)^3\right] = 2{,}782{,}000 \text{ in.}^4 ,$$

$$I_{\substack{\text{ACI T-beam} \\ \text{ACI 349-85, 8.10.4}}} = \frac{1}{12} 24(90)^3 - 2\left[\frac{1}{12} 9(78)^3\right] = 746{,}000 \text{ in.}^4 ,$$

$$I_{\substack{\text{neglect} \\ \text{end walls}}} = \frac{1}{12} 6(90)^3 = 364{,}000 \text{ in.}^4 .$$

$$I_{\text{ASCE 4-86}} = \frac{1}{12} 66\,(90)^3 - 2\left[\frac{1}{12} 30\,(78)^3\right] = 1{,}637{,}000 \text{ in.}^4 .$$

IV. CONCLUSIONS

The following conclusions were made based on the results of the floor response spectra matching for the various structures.

1. Linear response spectra techniques applied to the analytical responses generated with lumped-mass models of the structures did an excellent job of predicting the floor response spectra generated from experimentally measured response data. These predictions required modifications in the stiffness and damping from currently used design and analysis practice. The linear response spectra techniques continued to work well even after the structures were known to have sustained significant damage in previous simulated seismic tests as is evident in the calculations with CERL-1 during the 13.6-g's input.
2. The stiffness values that provide the best match are significantly lower than current design criteria would predict even if end walls were neglected.

3. At higher input levels, stiffness must be further reduced to obtain an accurate match.
4. In order to obtain an accurate match, damping values must be in the 6%-10% range at the low-level excitations and must be increased to as high as 35% when the damaged structure receives severe seismic loading after sustaining previous seismic damage.
5. Damping has a greater effect on peaks in the response spectra caused by resonance than it does on peaks caused by a surge in the energy content of the input signal.
6. For a multidegree-of-freedom (MDOF) system, a good match with the measured response spectra was obtained by progressively increasing the damping in the lower stories.
7. For MDOF systems, the damping in the bottom floor plays a major role in controlling the system response. The structures seem relatively insensitive to the damping values associated with the upper floors.
8. For MDOF systems, it is not clear that there is a unique set of damping values that provide the best match to the measured response spectra as is evident in the three "best estimates" of the Sandia structures response to the 1.27-g's seismic input. In general, the analytical model that gives the best overall match tends to overestimate the bottom floor response and underestimate the top floor response.

The fact that the reduced-stiffness linear models accurately predict the response of the damaged concrete structures is consistent with the response observed during static cyclic testing of large shear wall elements as discussed in Ref. 8. During these tests it was observed that, after a structure cracked, the subsequent cycles of response were linear with a reduced stiffness. This response was repeatable until load levels were obtained that introduced more cracking and further reduced the stiffness of the structure. After the additional cracking was introduced, the structures again responded in a linear manner but with an even further reduction in stiffness. Therefore, if a damaged structure was subjected to seismic inputs that would not introduce further damage, it would be expected that a reduced-stiffness linear model would accurately predict the structure's dynamic response. The 1940 El Centro earthquake, which was simulated in all tests analyzed, has its peak amplitude response at the beginning of the signal. If damage is caused by this portion

of the signal, most of the response will once again be in a reduced-stiffness linear manner. It is felt that, in this situation, the modified linear models will once more predict the response of the structure because of the nature of the input signal; most likely, they would not do the same for arbitrary inputs.

V. REFERENCES

1. E. G. Endebrock, R. C. Dove, and C. A. Anderson, "Margins to Failure--Category I Structures Program: Background and Experimental Plan," Los Alamos National Laboratory report LA-09030-MS, NUREG/CR-2347 (December 1981).

2. E. G. Endebrock, R. C. Dove, and W. E. Dunwoody, "Analysis and Tests on Small-Scale Shear Walls--FY 82 Final Report," Los Alamos National Laboratory report LA-10443-MS, NUREG/CR-4274 (September 1985).

3. R. C. Dove, J. G. Bennett, C. R. Farrar, and C. A. Anderson, "Seismic Category I Structures Program Final Report, FY 1983-84," Los Alamos National Laboratory report LA-11013-MS, NUREG/CR-4924 (September 1987).

4. R. C. Dove and J. G. Bennett, "Scale Modeling of Reinforced Concrete Category I Structures Subjected to Seismic Loads," Los Alamos National Laboratory report LA-10624-MS, NUREG/CR-4474 (January 1986).

5. J. G. Bennett, R. C. Dove, W. E. Dunwoody, E. G. Endebrock, C. R. Farrar, and P. Goldman, "Simulated Seismic Tests on 1/42- and 1/14-Scale Category I, Auxiliary Building," Los Alamos National Laboratory report LA-11093-MS, NUREG/CR-4987 (October 1987).

6. J. G. Bennett, R. C. Dove, W. E. Dunwoody, C. R. Farrar, and P. Goldman, "The Seismic Category I Structures Program: Results for FY 1985," Los Alamos National Laboratory report LA-11117-MS, NUREG/CR-4998 (December 1987).

7. J. G. Bennett, R. C. Dove, W. E. Dunwoody, C. R. Farrar, and P. Goldman, "The Seismic Category I Structures Program: Results for FY 1986," Los Alamos National Laboratory report LA-11377-MS, NUREG/CR-5182 (September 1988).

8. C. R. Farrar, "Dynamic Properties of Reinforced Concrete Shear Walls," Ph.D. thesis, The University of New Mexico (1988).

9. Committee on Nuclear Standards, Structural Analysis and Design of Nuclear Plant Facilities (A.S.C.E., New York, 1980), pp. 235-236.

10. Committee on Nuclear Standards, Seismic Analysis of Safety-Related Nuclear Structures (A.S.C.E., New York, 1987), p. 11.

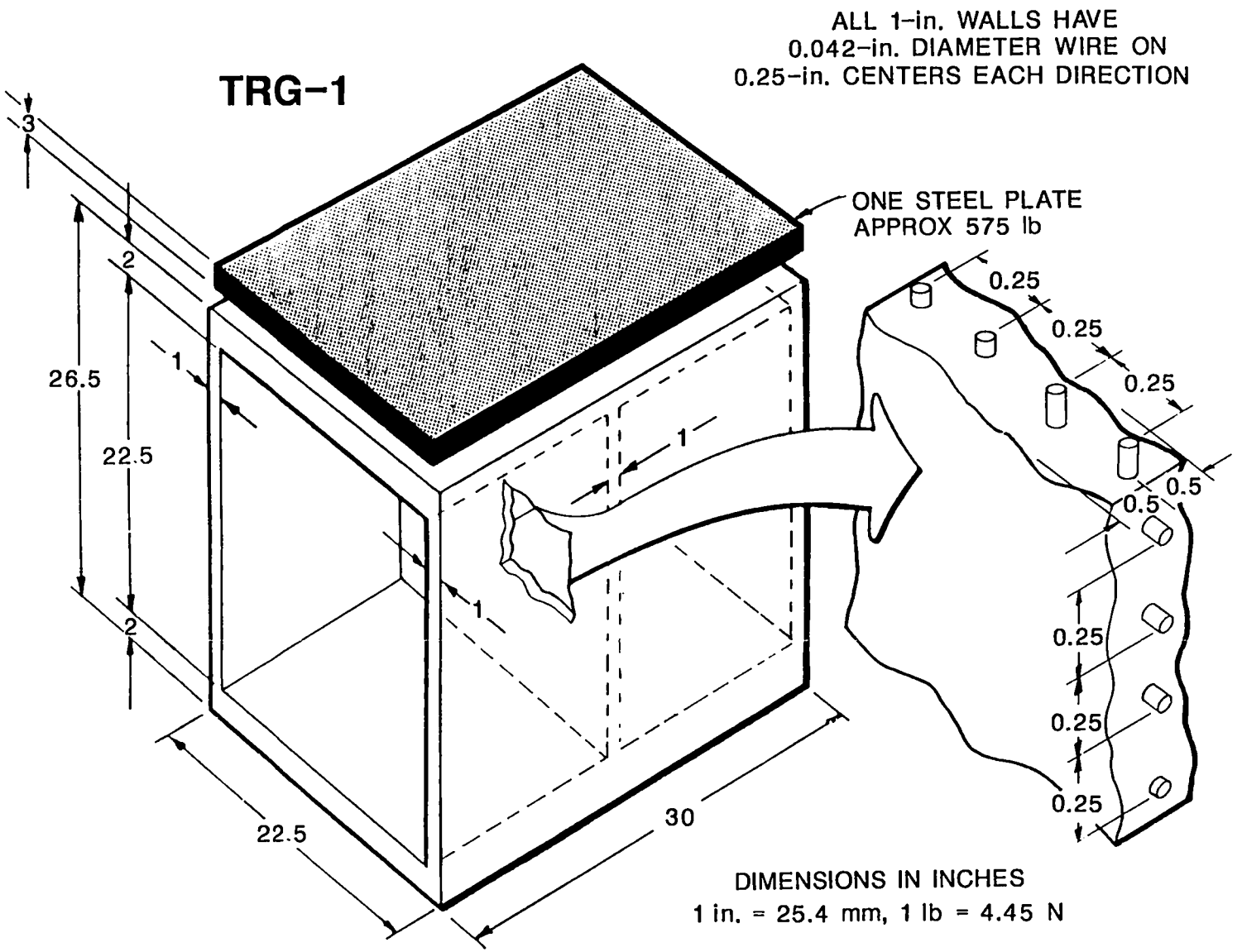

Fig. 1. The TRG-1 structure.

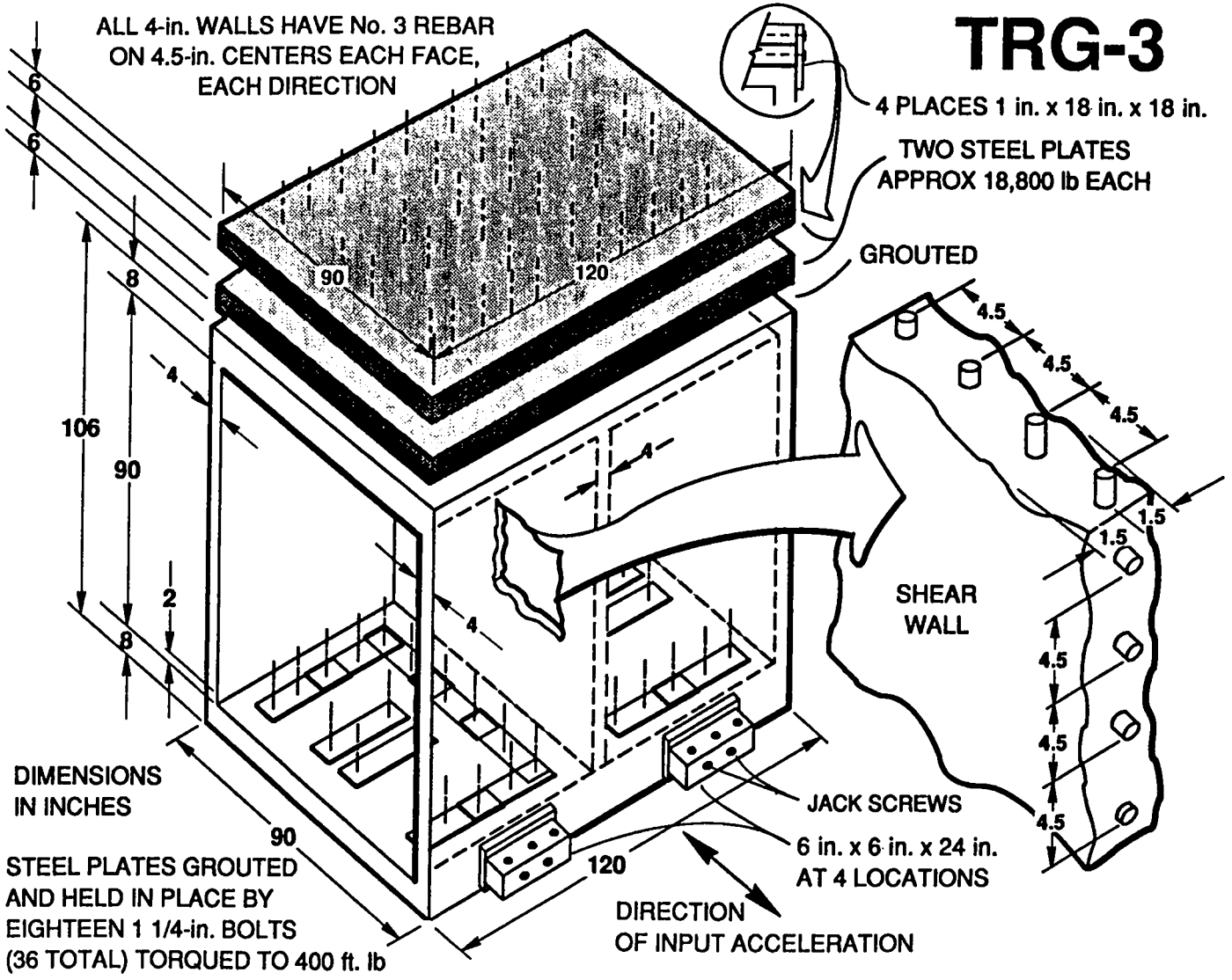

Fig. 2. The TRG-3 structure.

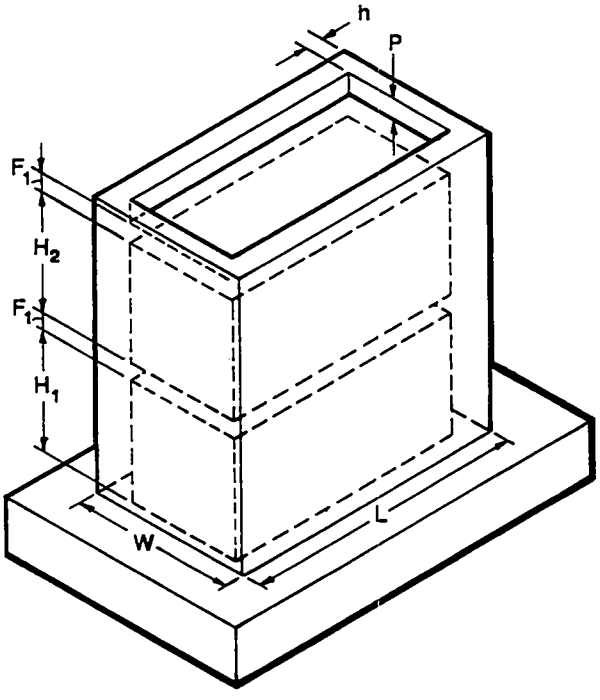

	h, F_1, F_2	W	L	H_1 & H_2	P	Wt/STORY *
1/30-SCALE	1 in.	10 in.	18 in.	7.25 in.	1 in.	47.7 lb
1/10-SCALE	3 in.	30 in.	54 in.	21.75 in.	3 in.	1286 lb
PROTOTYPE	30 in.	25 ft	45 in.	18.125 ft	30 in.	1,286,000 lb

*BASE NOT INCLUDED

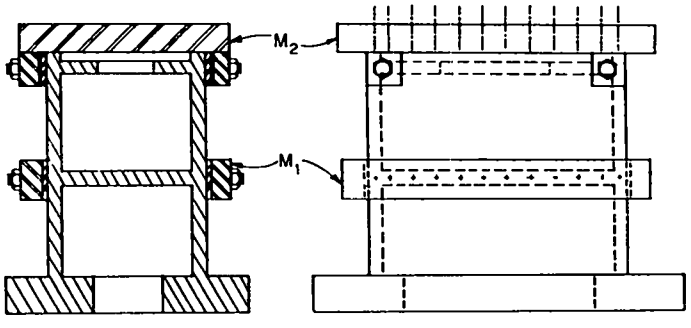

STRUCTURE	SCALE	M_1 (lbs)	M_2 (lbs)
3D-10-2	1/30	228	231
3D-10-2	1/30	228	231
3D-12-2	1/30	236	166
CERL 1	1/10	1285	1330
CERL 2	1/10	1285	906

Fig. 3. The CERL-1 structure.

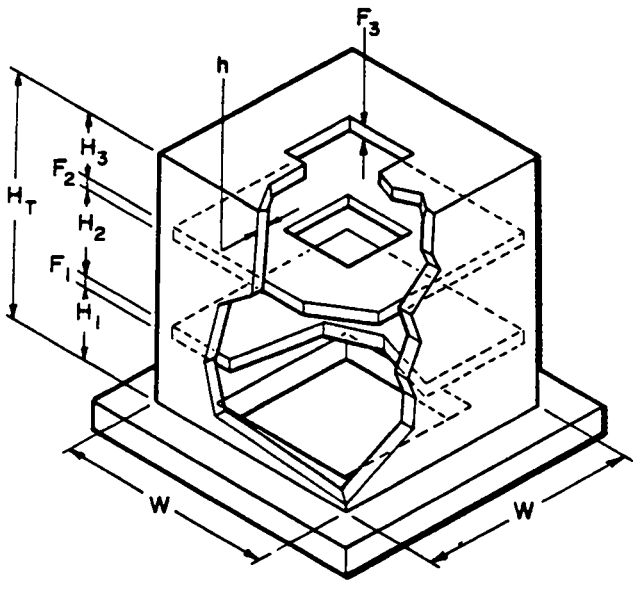

	h, F_1, F_2, F_3	W	H_1, H_2, H_3	Wt/STORY* (lb)
1/42 SCALE	1 in.	26 in.	10 in.	140
1/14 SCALE	3 in.	78 in.	30 in.	3780
PROTOTYPE	42 in.	1092 in.	42 in.	10,372,000

*BASE NOT INCLUDED

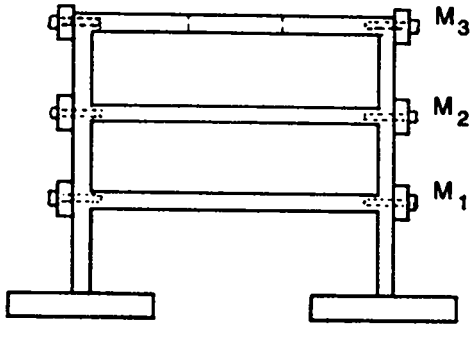

STRUCTURE	M_1 (lbs)	M_2 (lbs)	M_3 (lbs)
1/42-SCALE	500	460	395
1/14-SCALE	3334	3060	2631

Fig. 4. The SANDIA-1 structure.

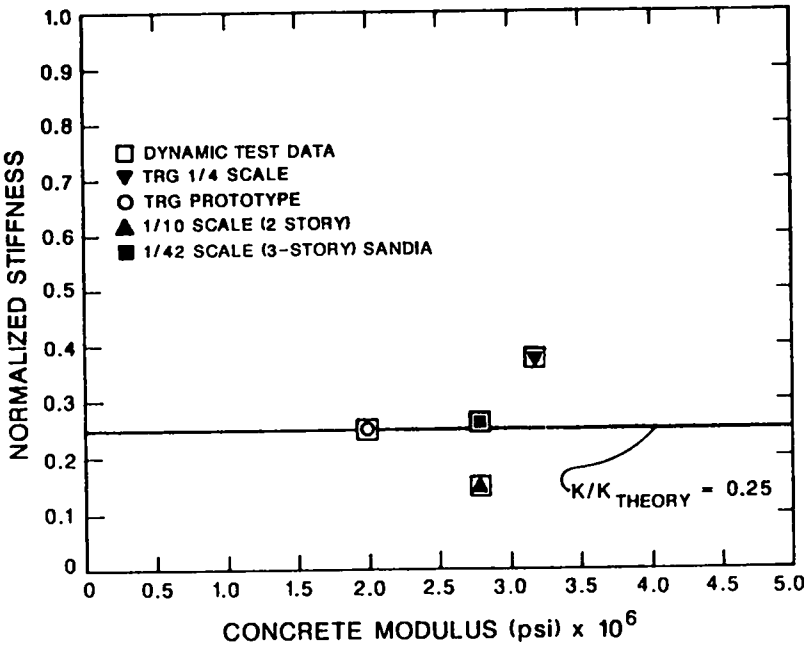

Fig. 5. Measured stiffness normalized to theoretical stiffness.

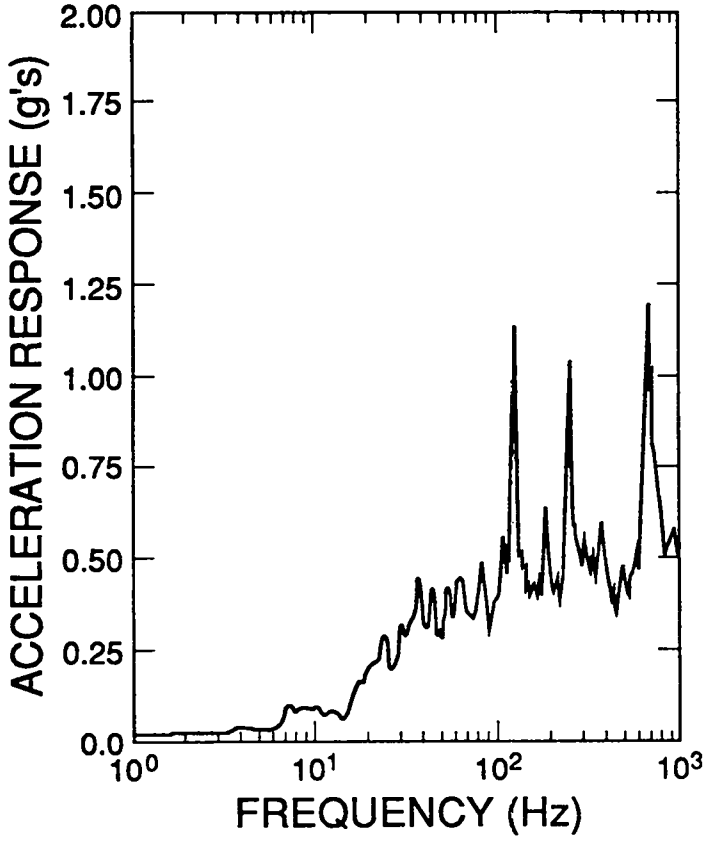

Fig. 6. TRG-1 base input at 0.211 g's and 2% damping.

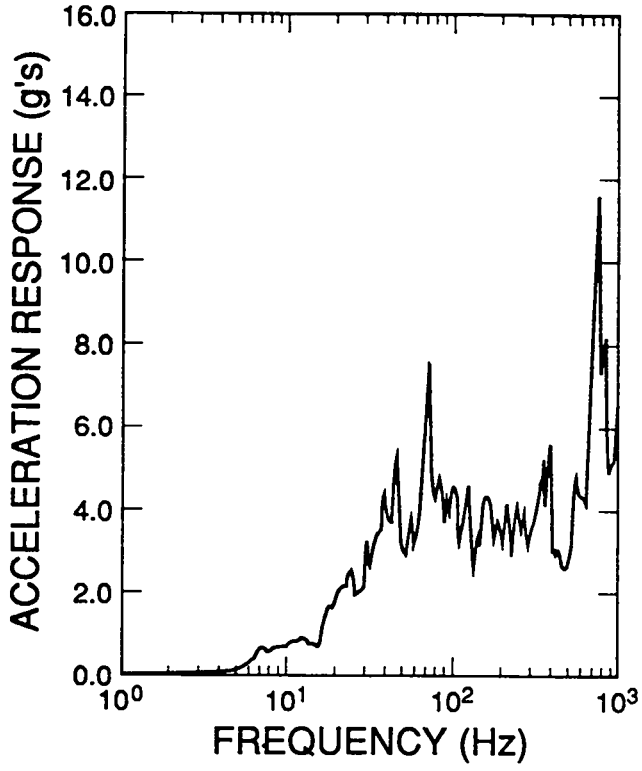

Fig. 7. TRG-1 base input at 2.54 g's and 2% damping.

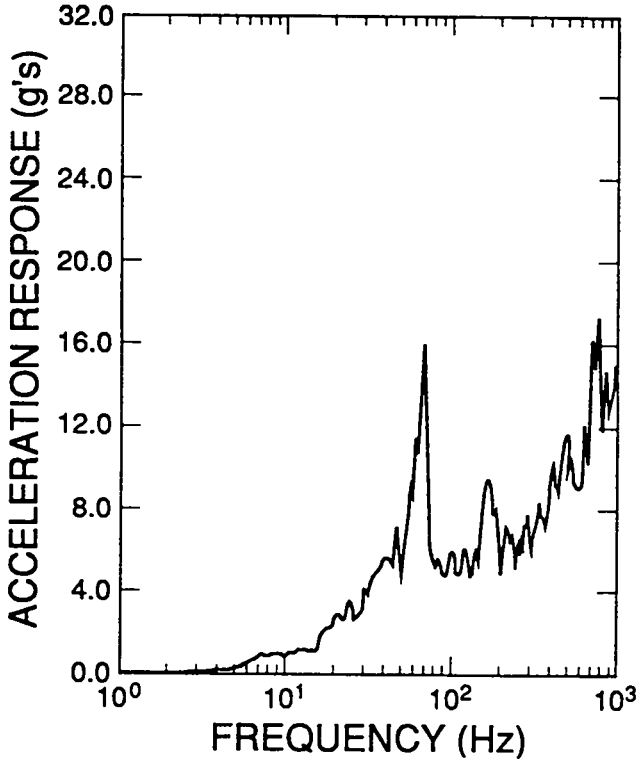

Fig. 8. TRG-1 base input at 7.23 g's and 2% damping.

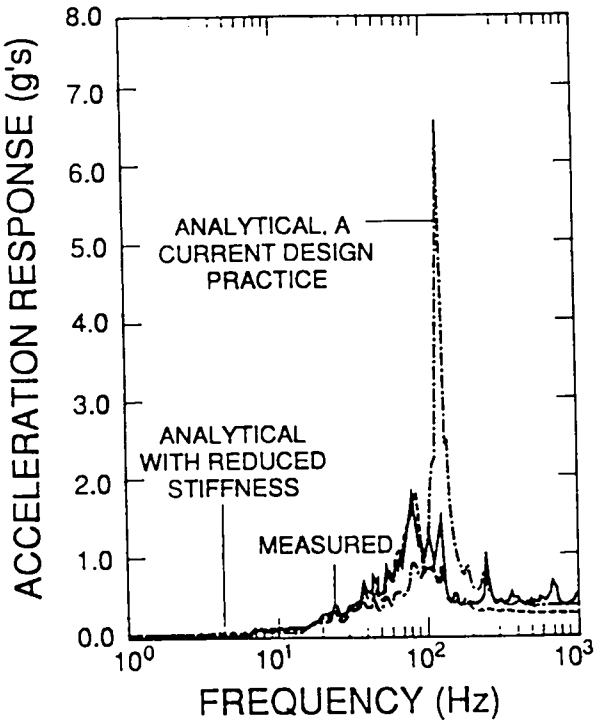

Fig. 9. Comparison of measured and analytical response spectra for TRG-1 at 0.211-g's input and 2% damping.

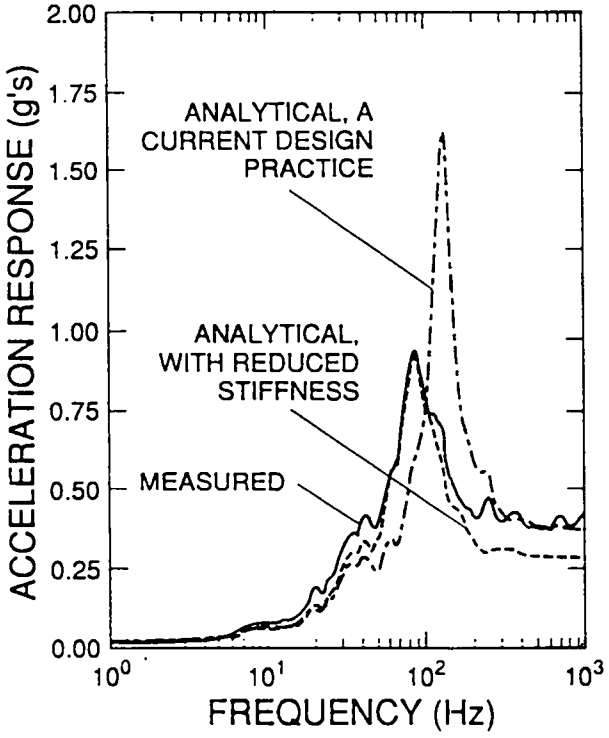

Fig. 10. Comparison of measured and analytical response spectra for TRG-1 at 0.211-g's input and 10% damping.

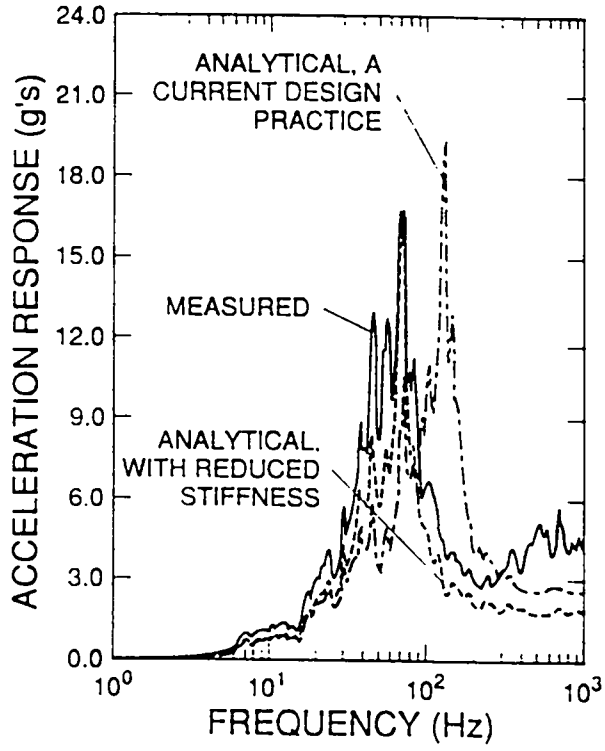

Fig. 11. Comparison of measured and analytical response spectra for TRG-1 at 2.54-g's input and 2% damping.

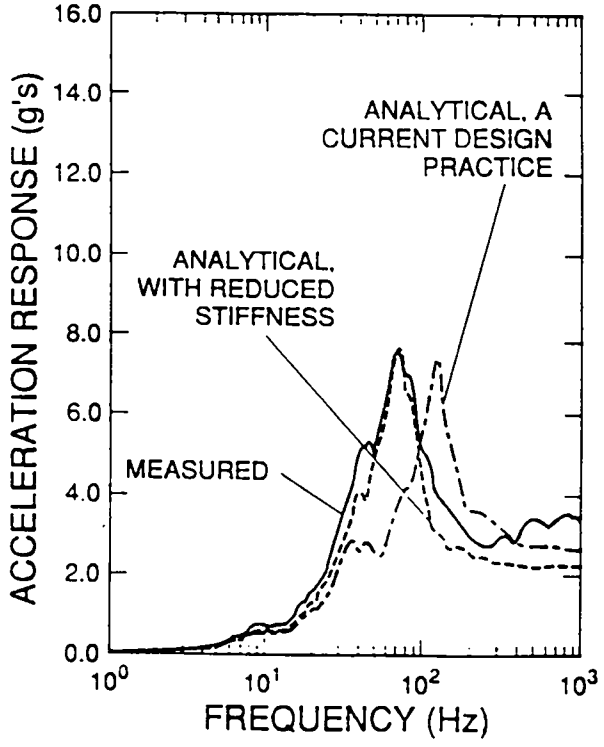

Fig. 12. Comparison of measured and analytical response spectra for TRG-1 at 2.54-g's input and 10% damping.

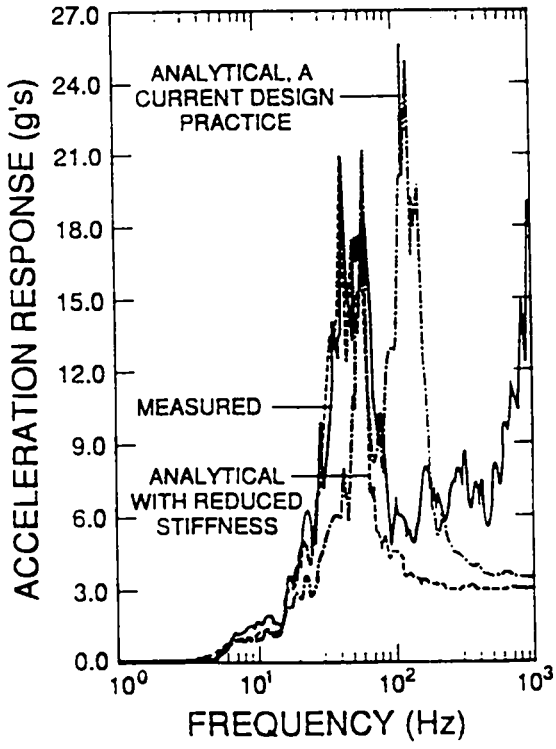

Fig. 13. Comparison of measured and analytical response spectra for TRG-1 at 7.23-g's input and 2% damping.

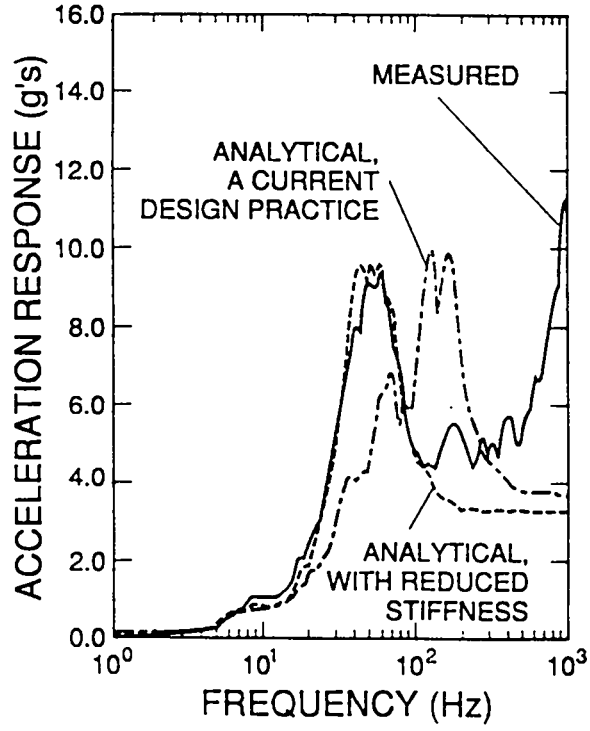

Fig. 14. Comparison of measured and analytical response spectra for TRG-1 at 7.23-g's input and 10% damping.

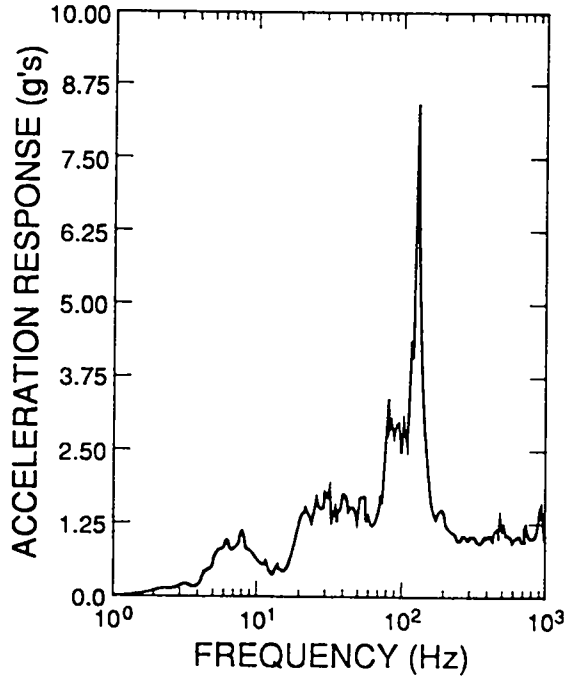

Fig. 15. TRG-3 base input at 0.88 g's and 2% damping.

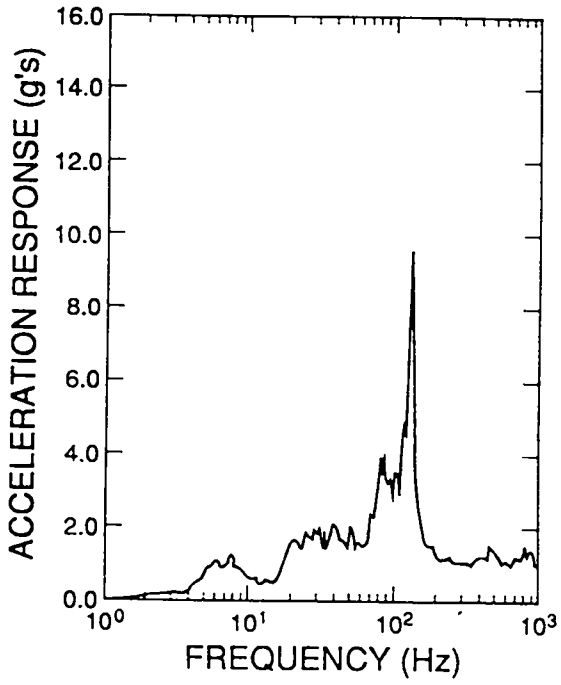

Fig. 16. TRG-3 base input at 0.99 g's and 2% damping.

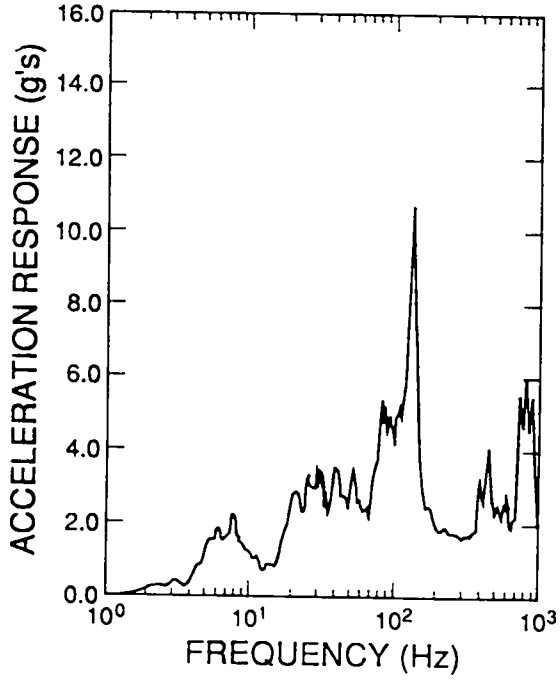

Fig. 17. TRG-3 base input at 1.65 g's and 2% damping.

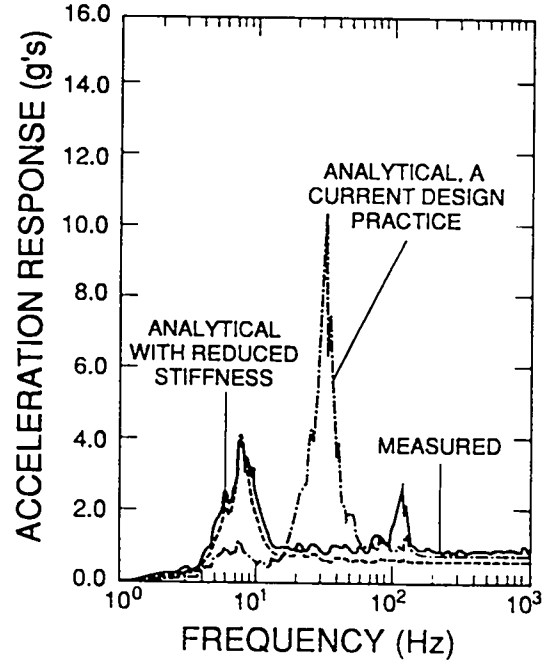

Fig. 18. Comparison of measured and analytical response spectra for TRG-3 at 0.88-g's input and 2% damping.

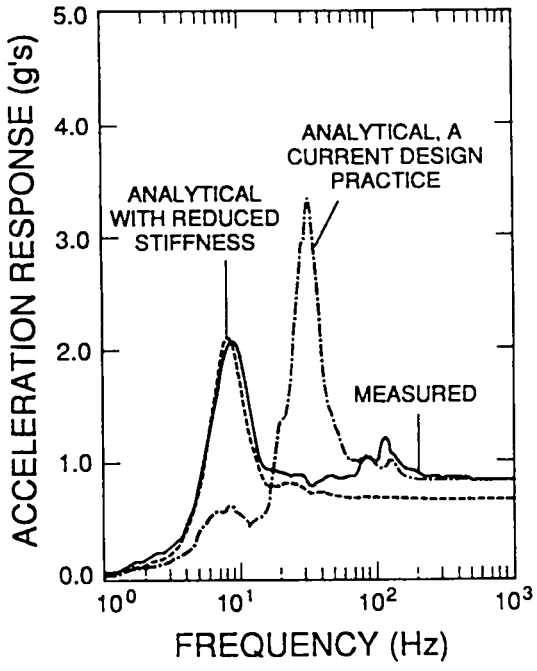

Fig. 19. Comparison of measured and analytical response spectra for TRG-3 at 0.88-g's input and 10% damping.

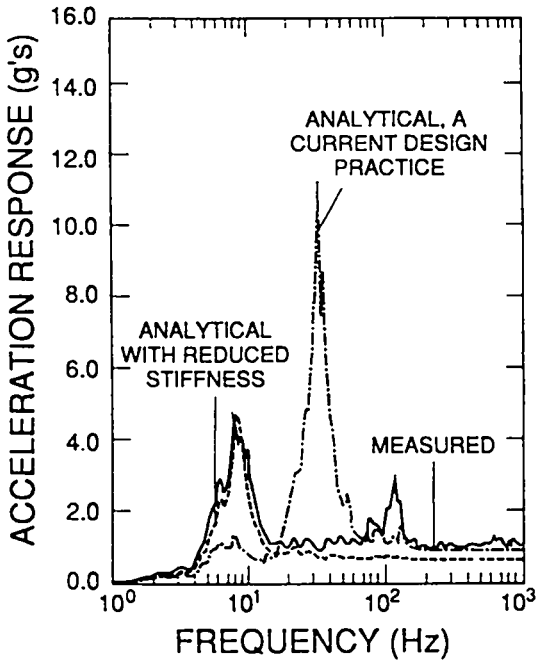

Fig. 20. Comparison of measured and analytical response spectra for TRG-3 at 0.99-g's input and 2% damping.

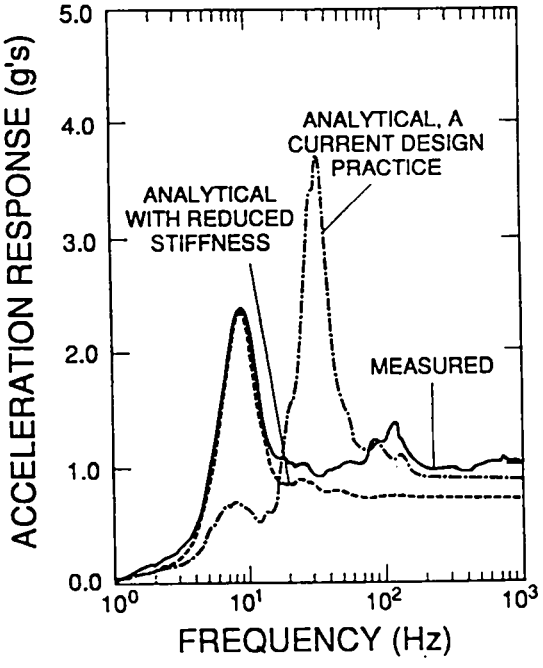

Fig. 21. Comparison of measured and analytical response spectra for TRG-3 at 0.99-g's input and 10% damping.

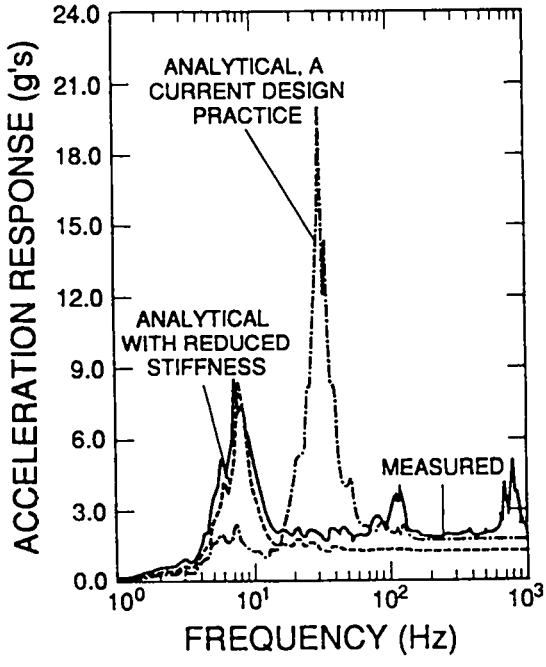

Fig. 22. Comparison of measured and analytical response spectra for TRG-3 at 1.65-g's input and 2% damping.

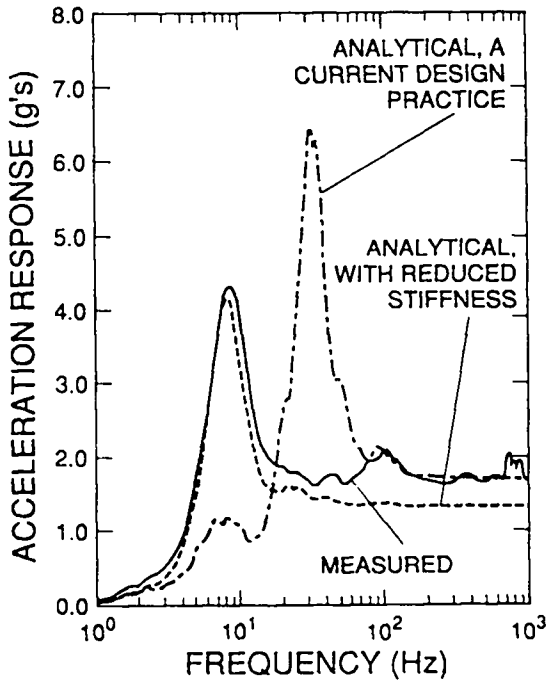

Fig. 23. Comparison of measured and analytical response spectra for TRG-3 at 1.65-g's input and 10% damping.

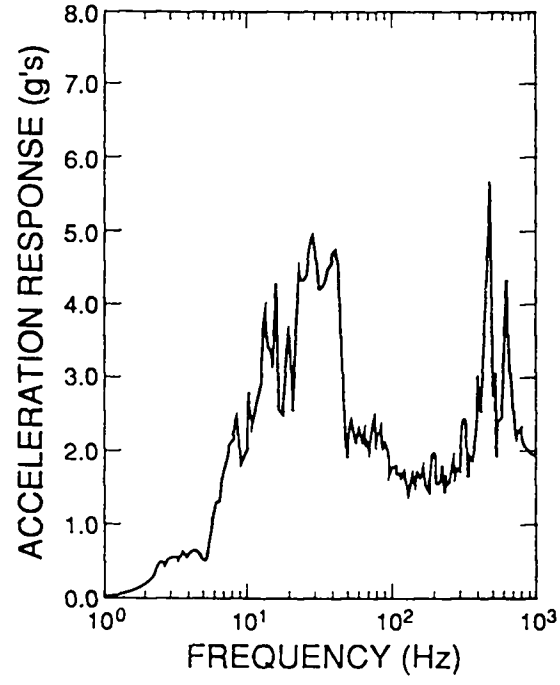

Fig. 24. CERL-1 base input at 1.88 g's and 2% damping.

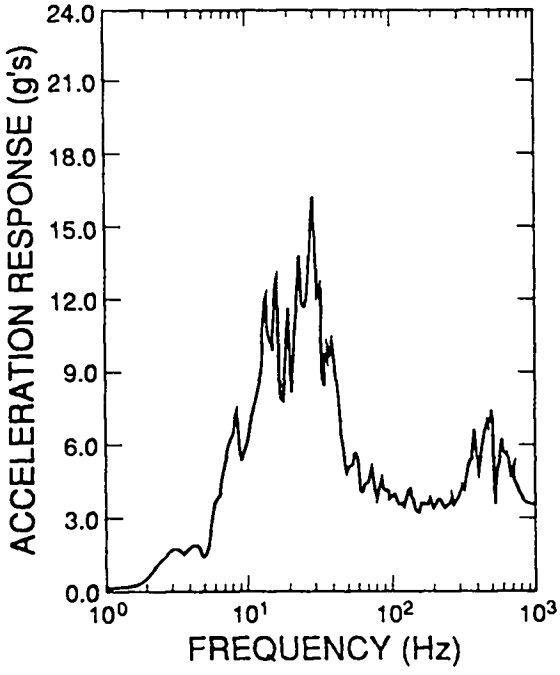

Fig. 25. CERL-1 base input at 3.53 g's and 2% damping.

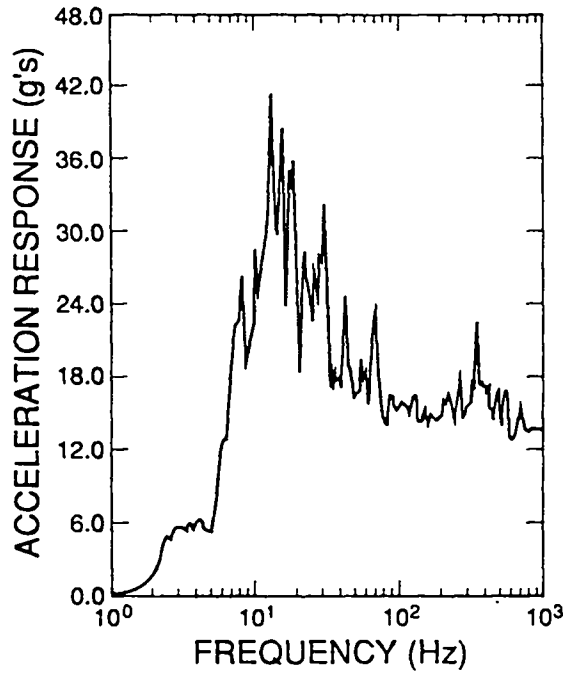

Fig. 26. CERL-1 base input at 13.66 g's and 2% damping.

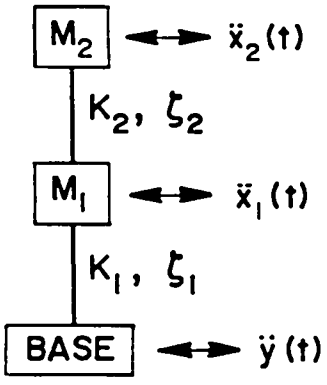

Fig. 27. Lumped-mass model of the CERL-1 structure.

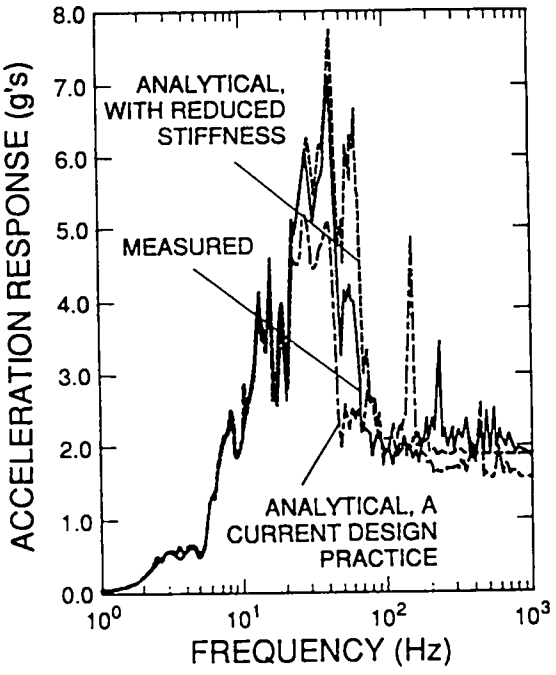

Fig. 28. Comparison of measured and analytical response spectra for CERL-1, Floor 1, at 1.88-g's input and 2% damping.

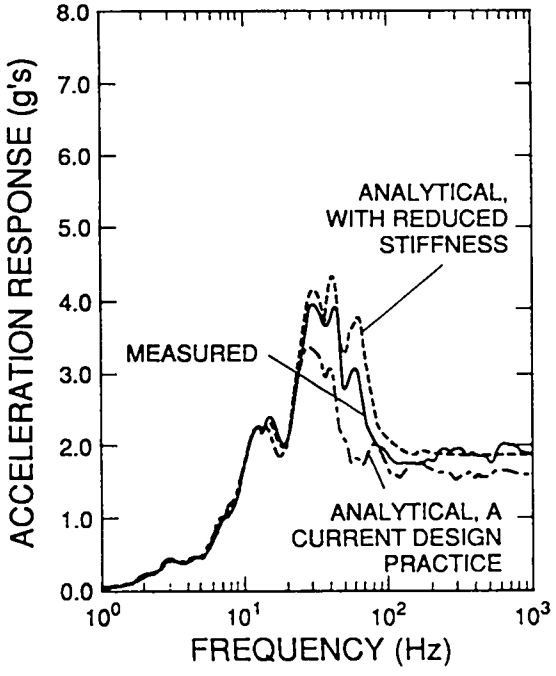

Fig. 29. Comparison of measured and analytical response spectra for CERL-1, Floor 1, at 1.88-g's input and 10% damping.

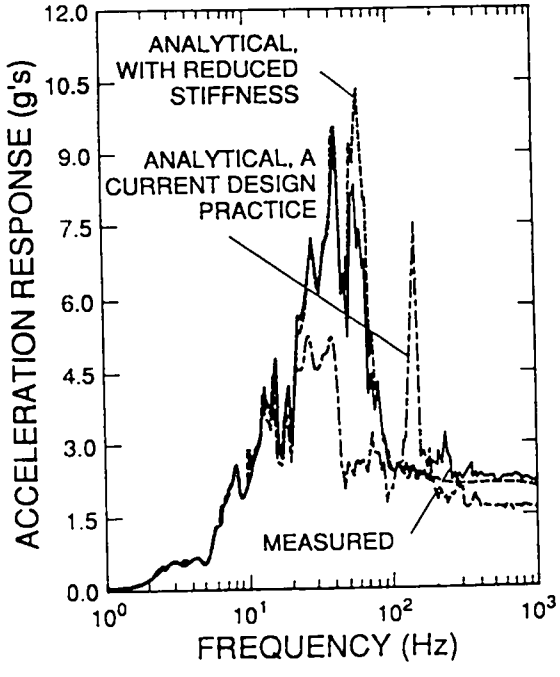

Fig. 30. Comparison of measured and analytical response spectra for CERL-1, Floor 2, at 1.88-g's input and 2% damping.

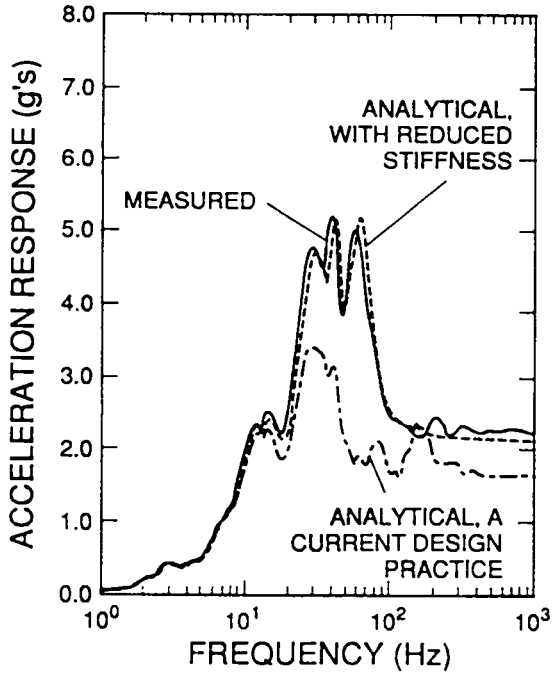

Fig. 31. Comparison of measured and analytical response spectra for CERL-1, Floor 2, at 1.88-g's input and 10% damping.

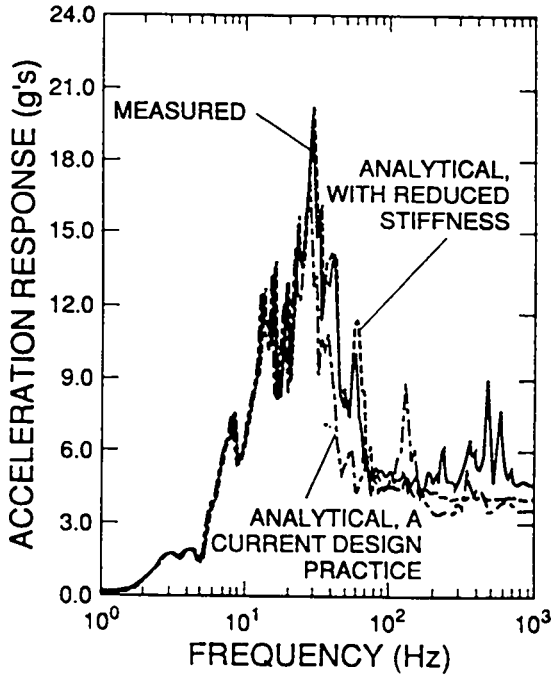

Fig. 32. Comparison of measured and analytical response spectra for CERL-1, Floor 1, at 3.53-g's input and 2% damping.

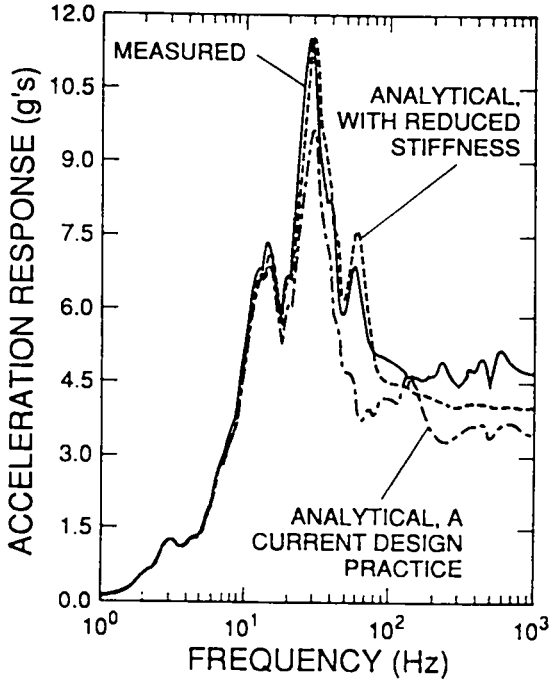

Fig. 33. Comparison of measured and analytical response spectra for CERL-1, Floor 1, at 3.53-g's input and 10% damping.

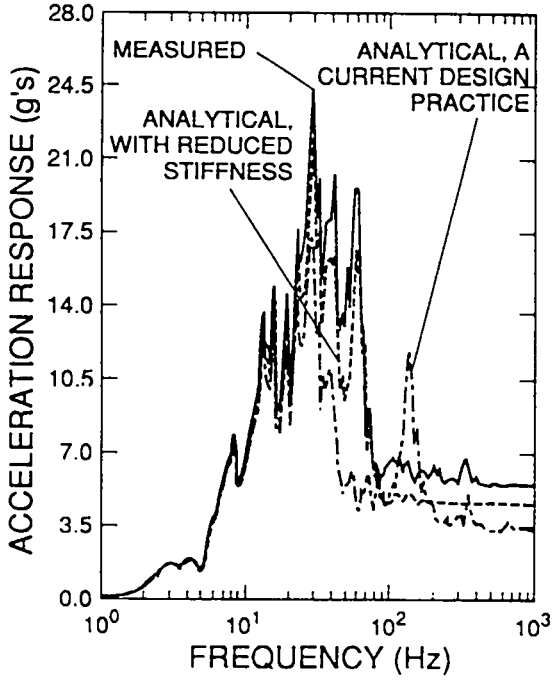

Fig. 34. Comparison of measured and analytical response spectra for CERL-1, Floor 2, at 3.53-g's input and 2% damping.

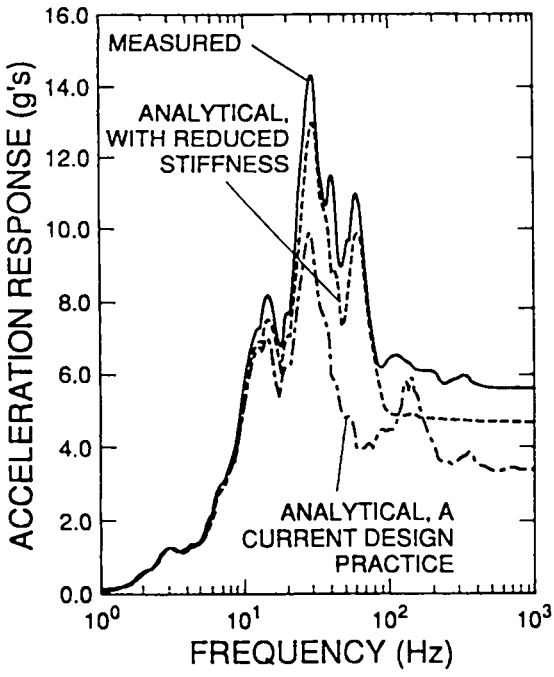

Fig. 35. Comparison of measured and analytical response spectra for CERL-1, Floor 2, at 3.53-g's input and 10% damping.

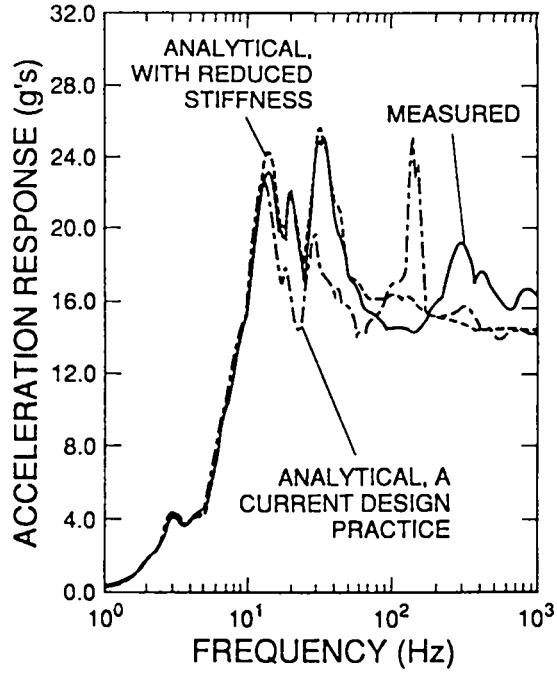

Fig. 36. Comparison of measured and analytical response spectra for CERL-1, Floor 1, at 13.66-g's input and 2% damping.

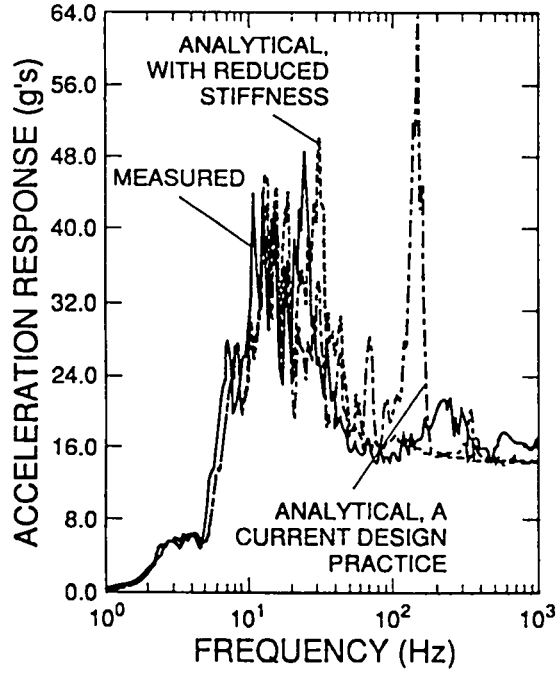

Fig. 37. Comparison of measured and analytical response spectra for CERL-1, Floor 1, at 13.66-g's input, and 10% damping.

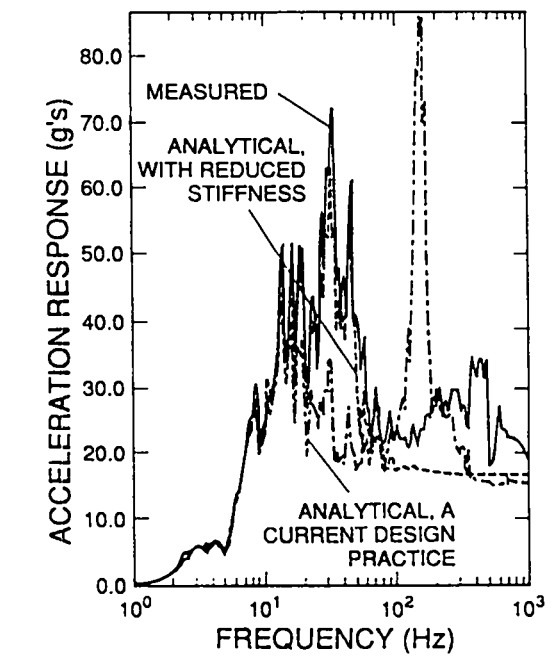

Fig. 38. Comparison of measured and analytical response spectra for CERL-1, Floor 2, at 13.66-g's input, and 2% damping.

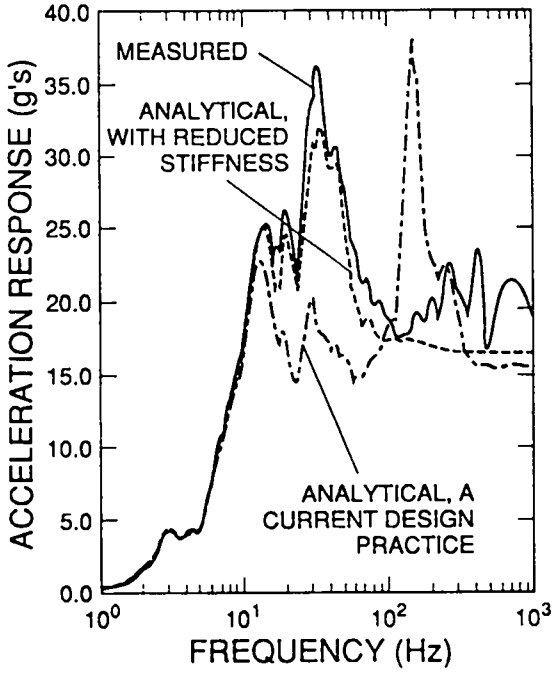

Fig. 39. Comparison of measured and analytical response spectra for CERL-1, Floor 2, at 13.66-g's input and 10% damping.

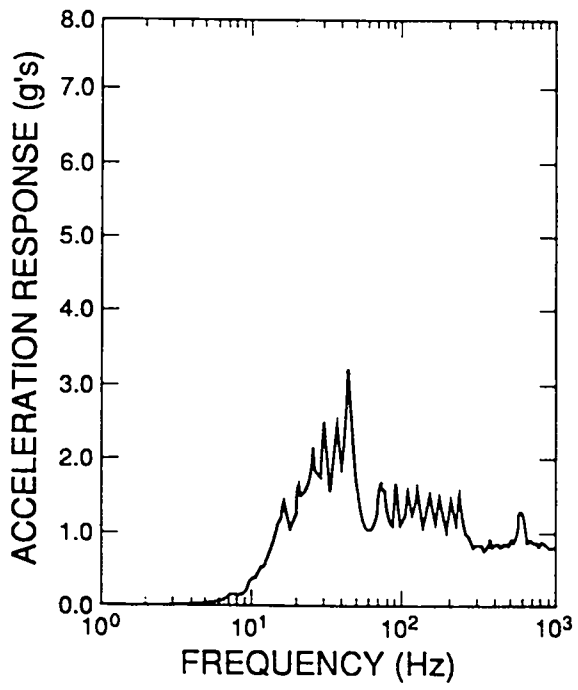

Fig. 40. SANDIA-1 base input at 0.65 g's and 2% damping.

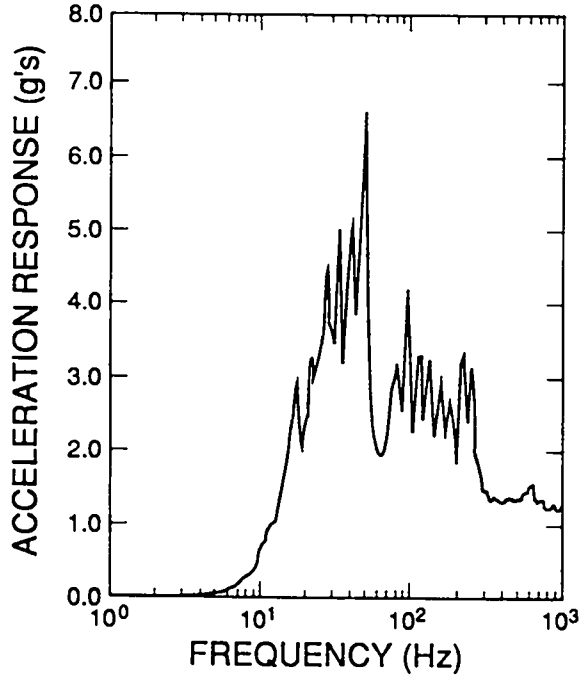

Fig. 41. SANDIA-1 base input at 1.27 g's and 2% damping.

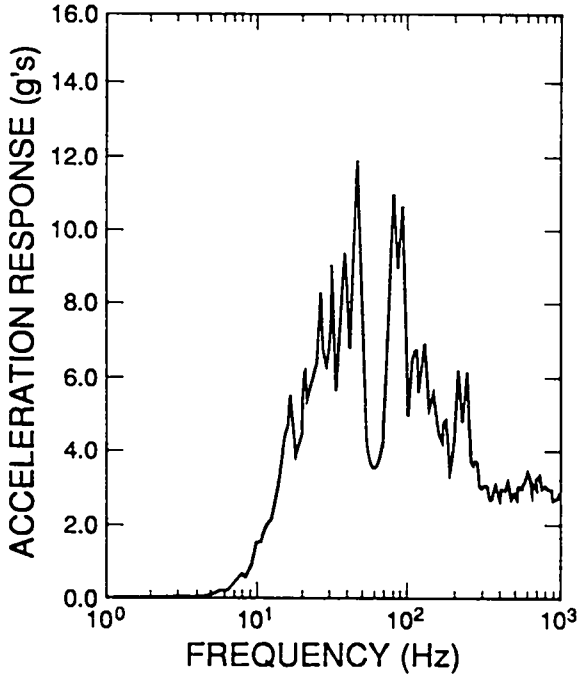

Fig. 42. SANDIA-1 base input at 2.83 g's and 2% damping.

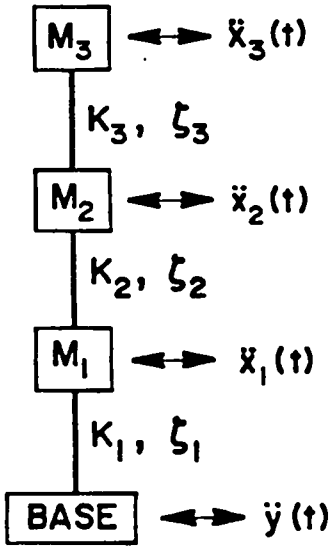

Fig. 43. Lumped-mass model of the SANDIA-1 structure.

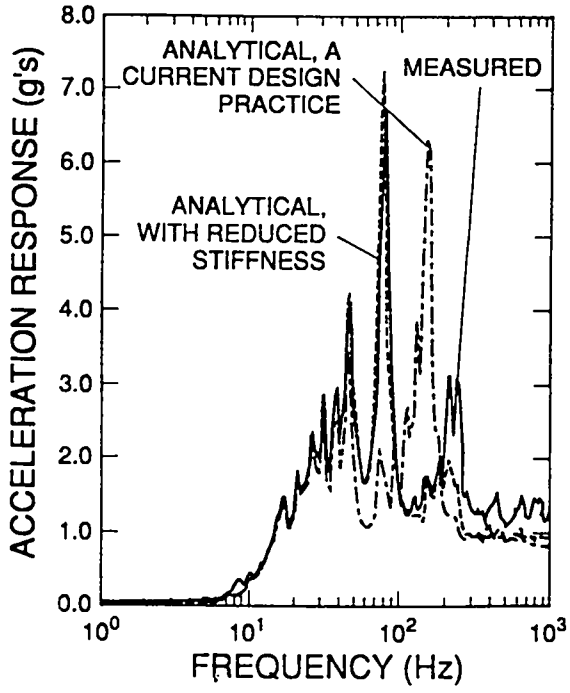

Fig. 44. Comparison of measured and analytical response spectra for SANDIA-1, Floor 1, at 0.65-g's input and 2% damping.

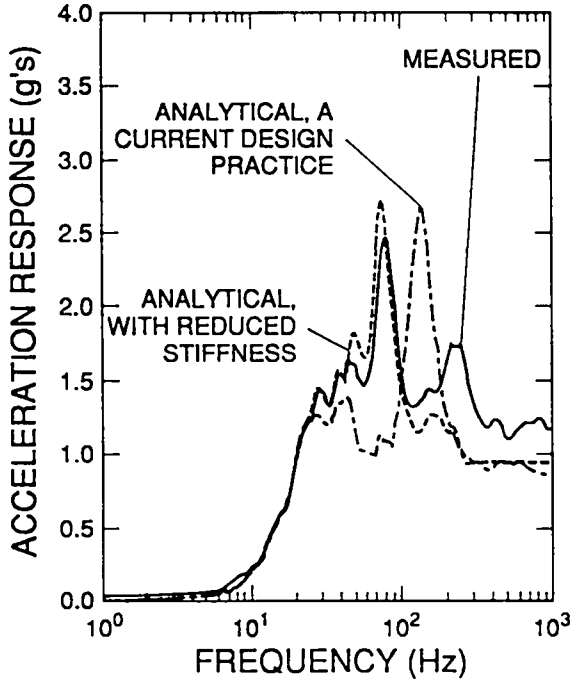

Fig. 45. Comparison of measured and analytical response spectra for SANDIA-1, Floor 1, at 0.65-g's input and 10% damping.

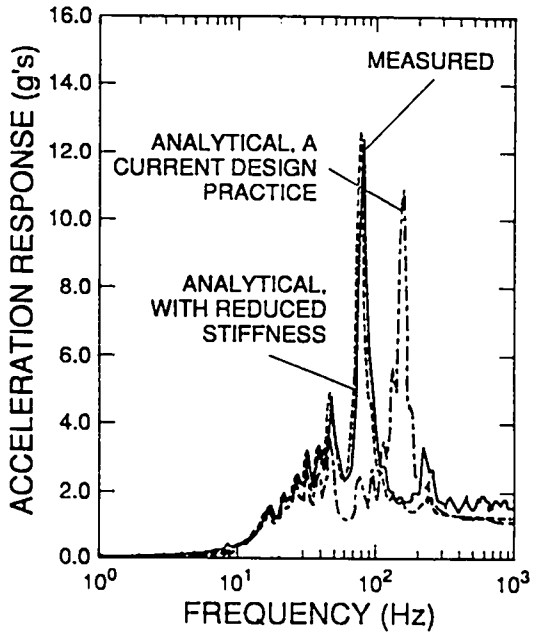

Fig. 46. Comparison of measured and analytical response spectra for SANDIA-1, Floor 2, at 0.65-g's input and 2% damping.

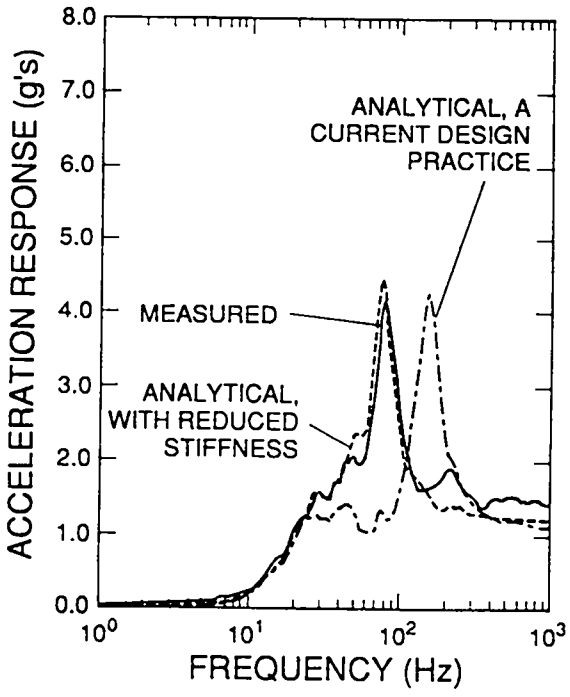

Fig. 47. Comparison of measured and analytical response spectra for SANDIA-1, Floor 2, at 0.65-g's input and 10% damping.

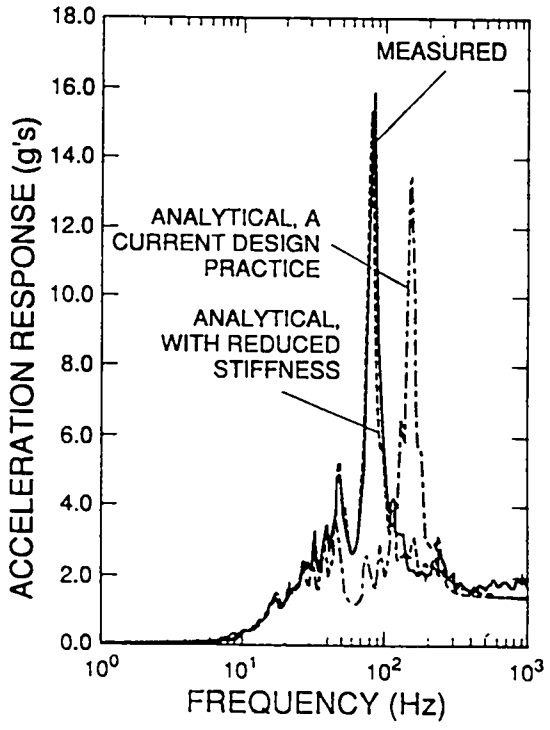

Fig. 48. Comparison of measured and analytical response spectra for SANDIA-1, Floor 3, at 0.65-g's input and 2% damping.

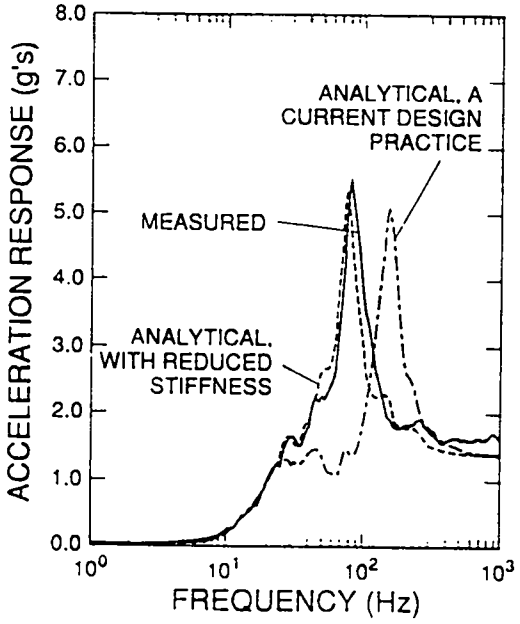

Fig. 49. Comparison of measured and analytical response spectra for SANDIA-1, Floor 3, at 0.65-g's input and 10% damping.

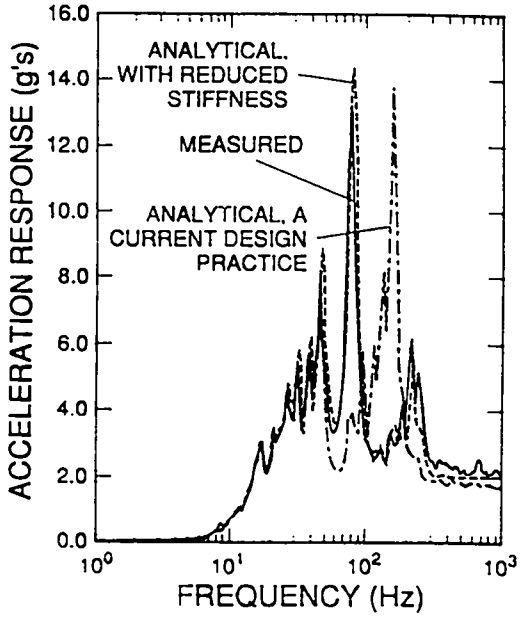

Fig. 50. Comparison of measured and analytical response spectra for SANDIA-1, Floor 1, at 1.27-g's input and 2% damping.

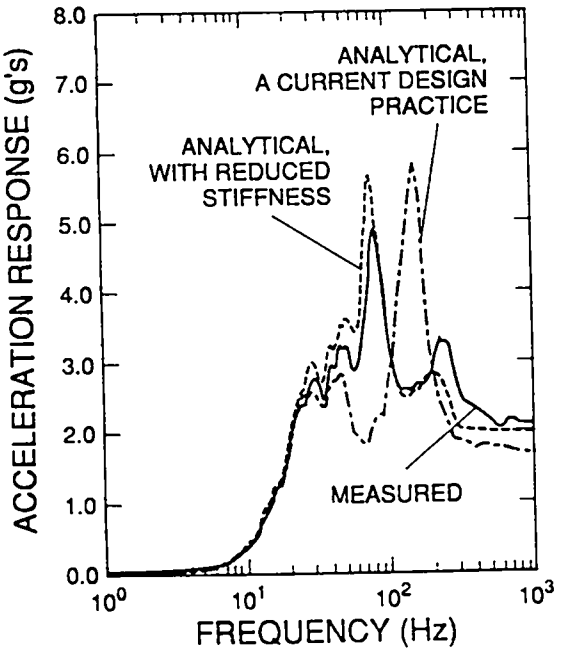

Fig. 51. Comparison of measured and analytical response spectra for SANDIA-1, Floor 1, at 1.27-g's input and 10% damping.

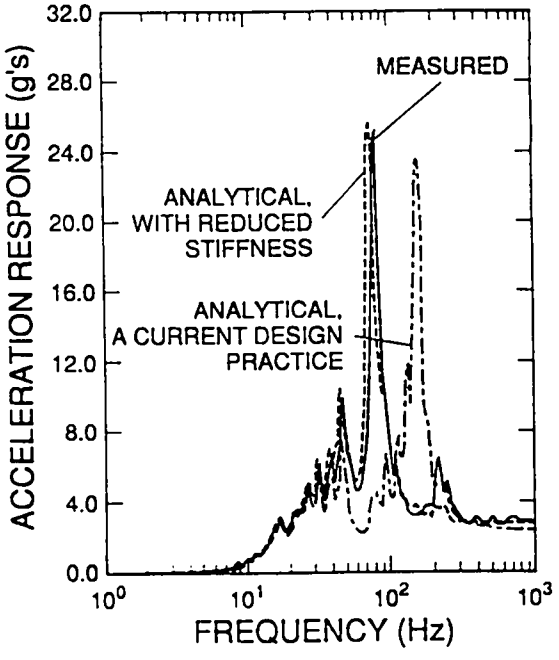

Fig. 52. Comparison of measured and analytical response spectra for SANDIA-1, Floor 2, at 1.27-g's input and 2% damping.

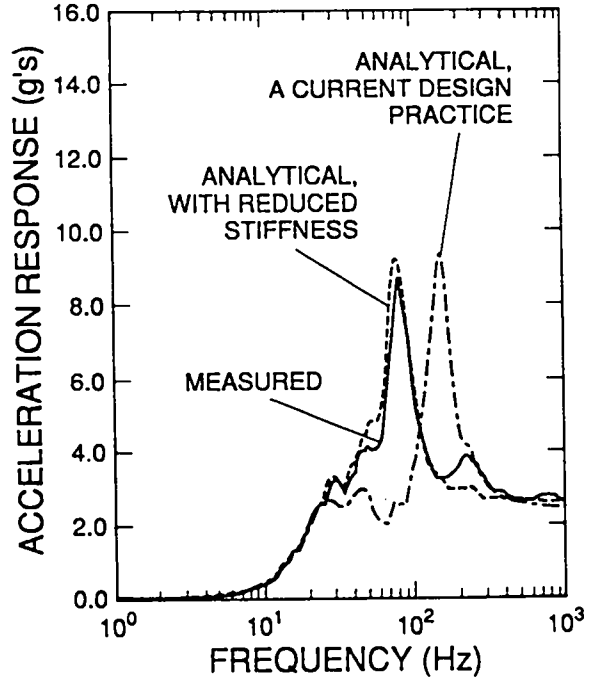

Fig. 53. Comparison of measured and analytical response spectra for SANDIA-1, Floor 2, at 1.27-g's input and 10% damping.

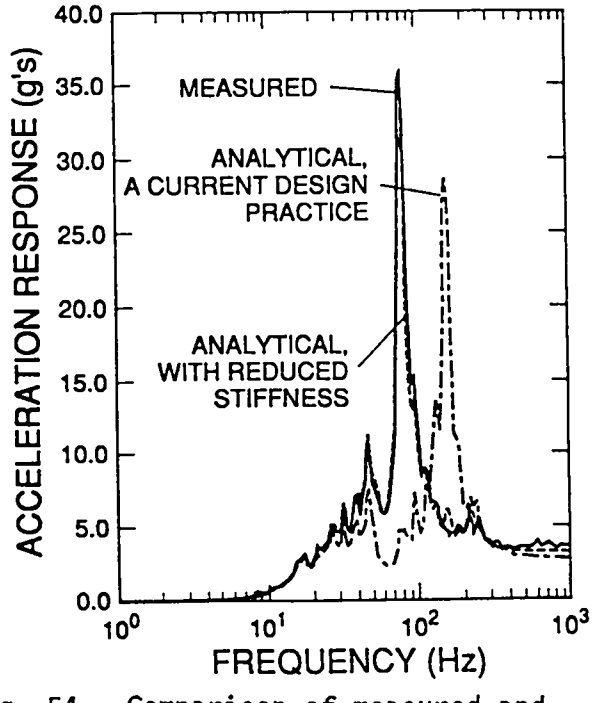

Fig. 54. Comparison of measured and analytical response spectra for SANDIA-1, Floor 3, at 1.27-g's input and 2% damping.

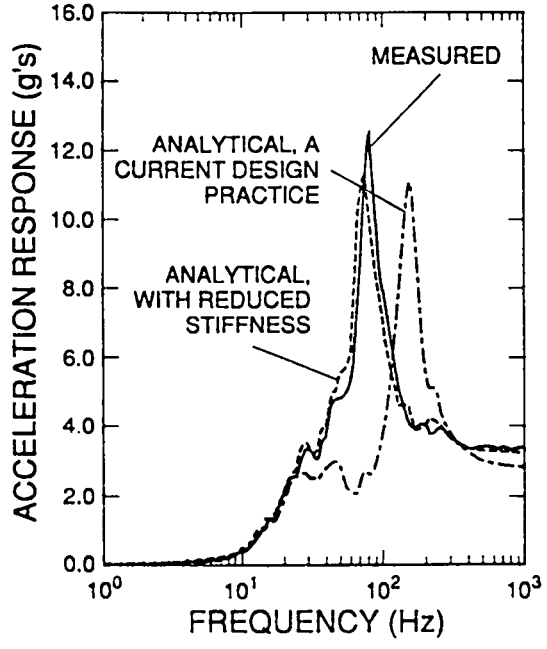

Fig. 55. Comparison of measured and analytical response spectra for SANDIA-1, Floor 3, at 1.27-g's input and 10% damping.

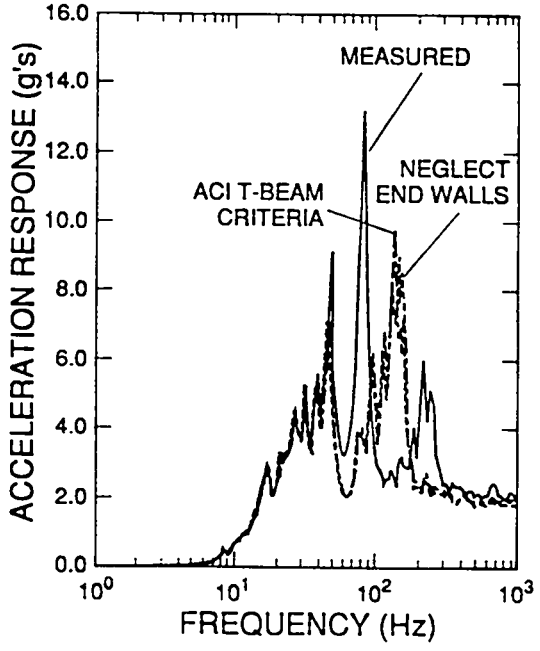

Fig. 56. Comparison of measured and analytical response spectra for SANDIA-1, Floor 1, at 1.27-g's input and 2% damping.

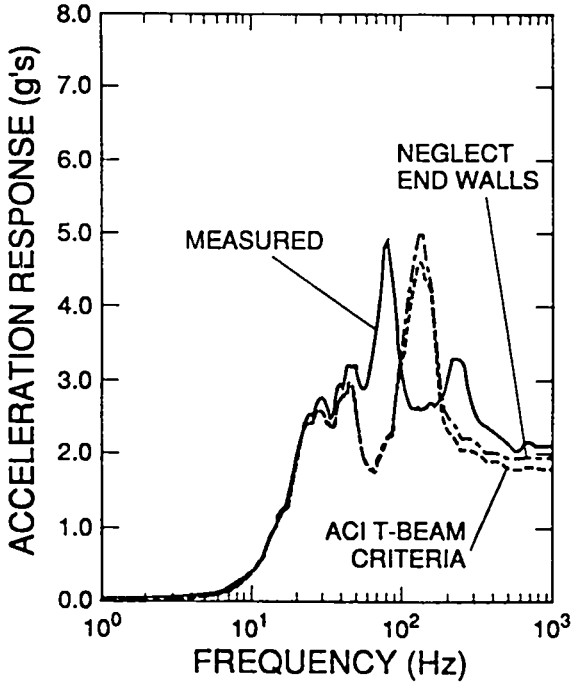

Fig. 57. Comparison of measured and analytical response spectra for SANDIA-1, Floor 1, at 1.27-g's input and 10% damping.

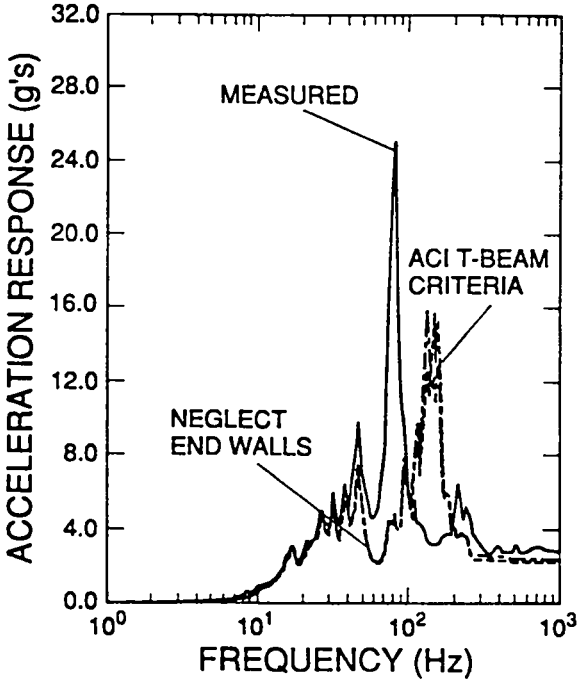

Fig. 58. Comparison of measured and analytical response spectra for SANDIA-1, Floor 2, at 1.27-g's input and 2% damping.

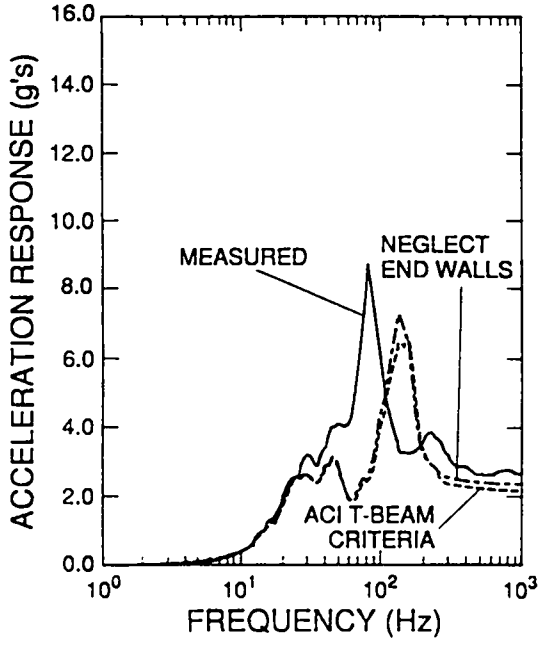

Fig. 59. Comparison of measured and analytical response spectra for SANDIA-1, Floor 2, at 1.27-g's input and 10% damping.

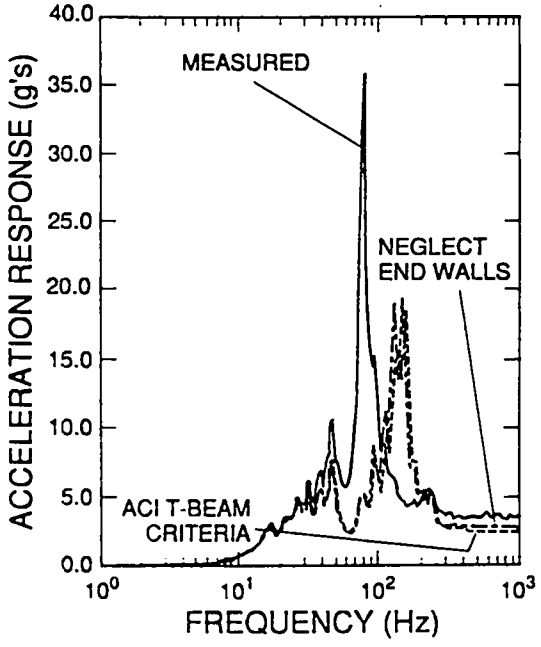

Fig. 60. Comparison of measured and analytical response spectra for SANDIA-1, Floor 3, at 1.27-g's input and 2% damping.

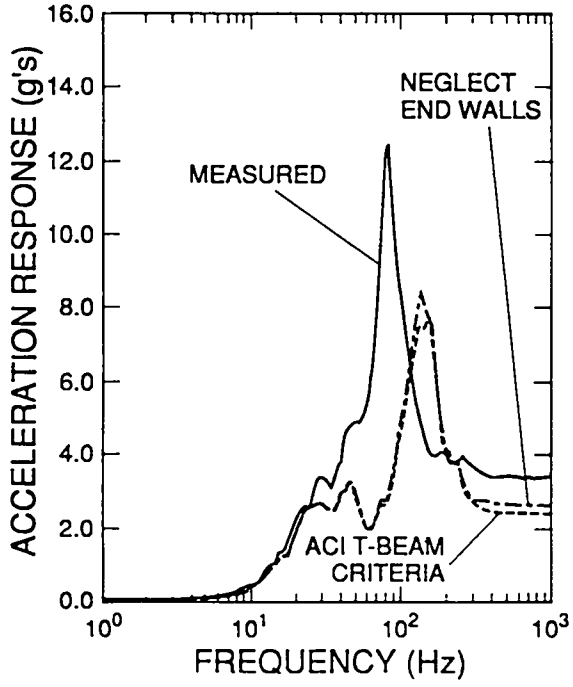

Fig. 61. Comparison of measured and analytical response spectra for SANDIA-1, Floor 3, at 1.27-g's input and 10% damping.

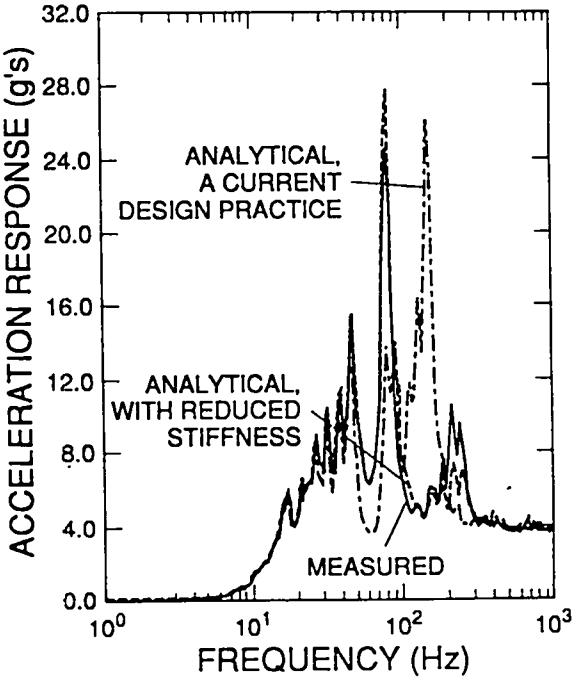

Fig. 62. Comparison of measured and analytical response spectra for SANDIA-1, Floor 1, at 2.83-g's input and 2% damping.

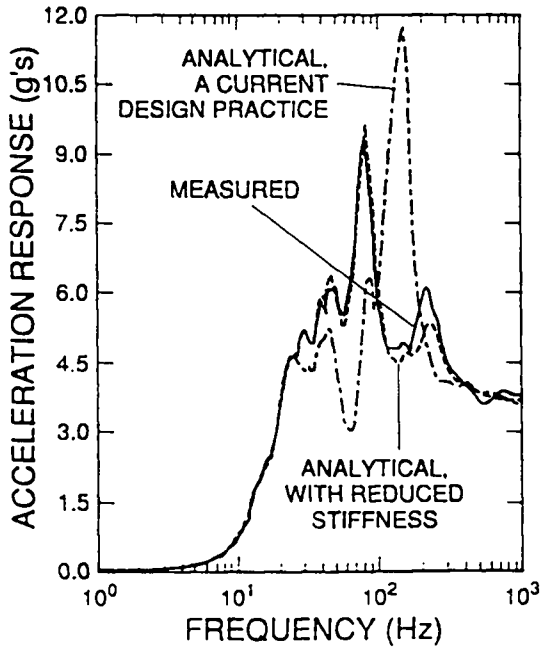

Fig. 63. Comparison of measured and analytical response spectra for SANDIA-1, Floor 1, at 2.83-g's input and 10% damping.

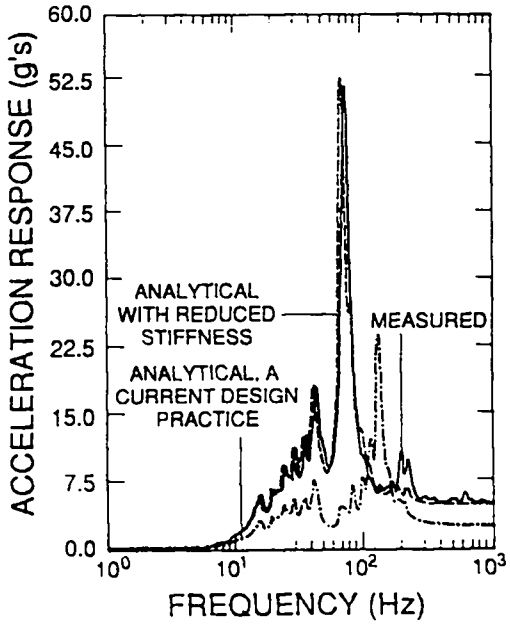

Fig. 64. Comparison of measured and analytical response spectra for SANDIA-1, Floor 2, at 2.83-g's input and 2% damping.

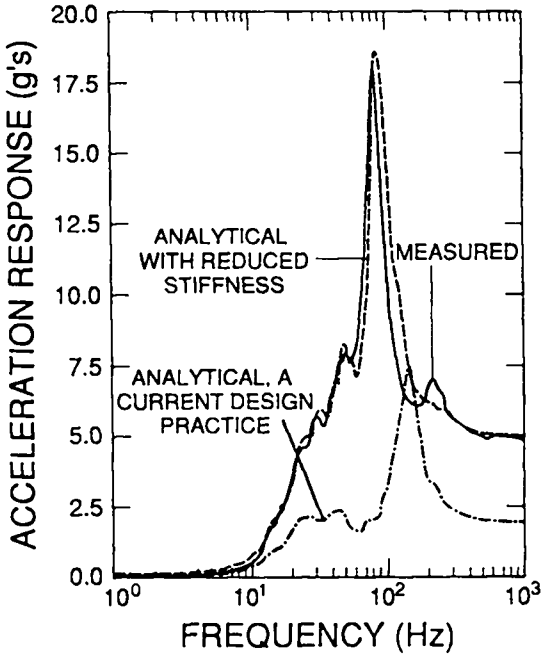

Fig. 65. Comparison of measured and analytical response spectra for SANDIA-1, Floor 2, at 2.83-g's input and 10% damping.

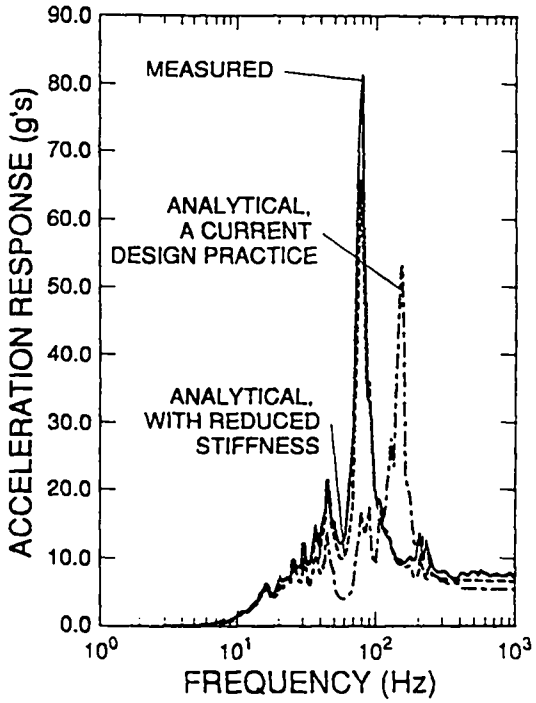

Fig. 66. Comparison of measured and analytical response spectra for SANDIA-1, Floor 3, at 2.83-g's input and 2% damping.

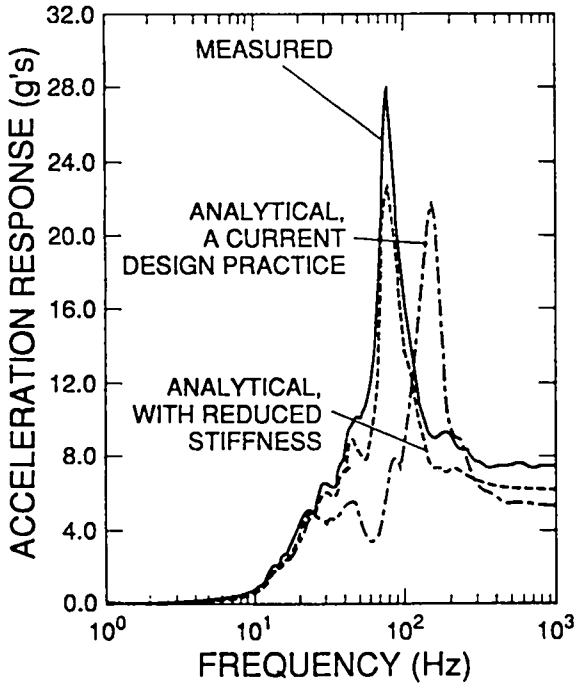

Fig. 67. Comparison of measured and analytical response spectra for SANDIA-1, Floor 3, at 2.83-g's input and 10% damping.

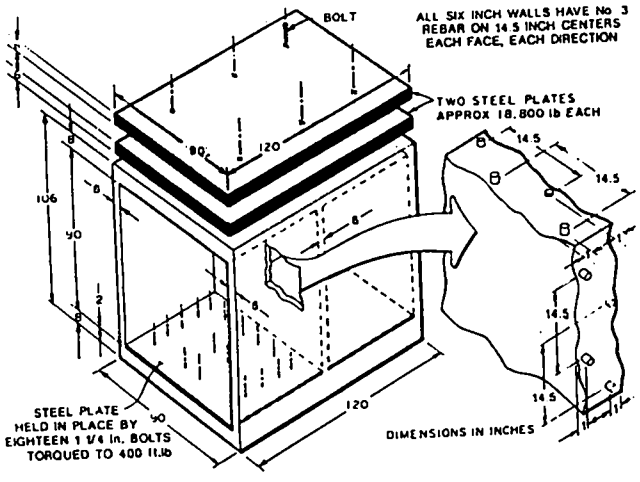

Fig. 68. The TRG-4 structure.

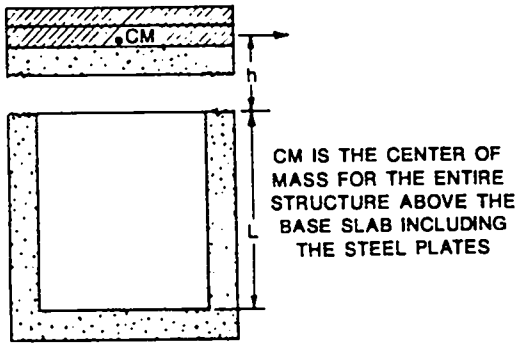

Fig. 69. Free-body diagram of TRG-type structure.

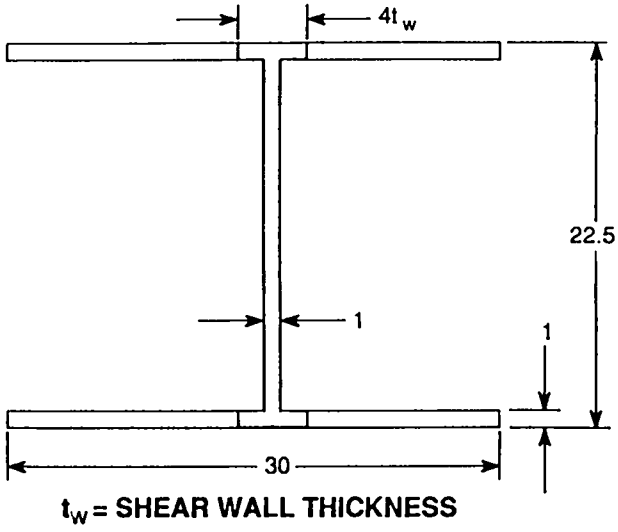

Fig. 70. ACI T-beam criteria applied to TRG-1.

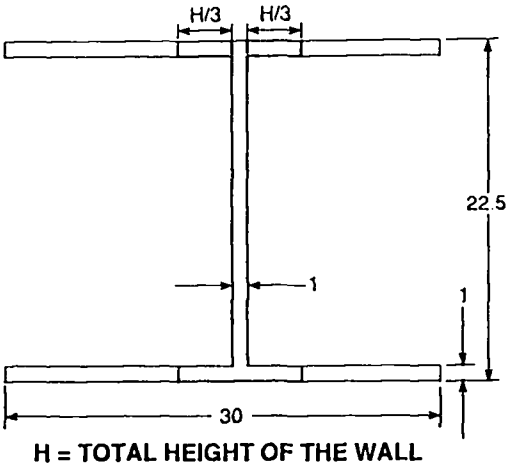

Fig. 71. ASCE method for assessing boundary element contribution to shear wall bending stiffness applied to TRG-1.

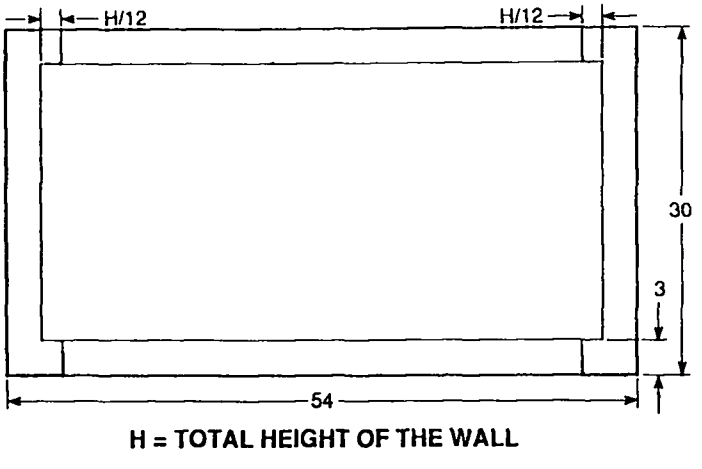

Fig. 72. ACI T-beam criteria applied to CERL-1.

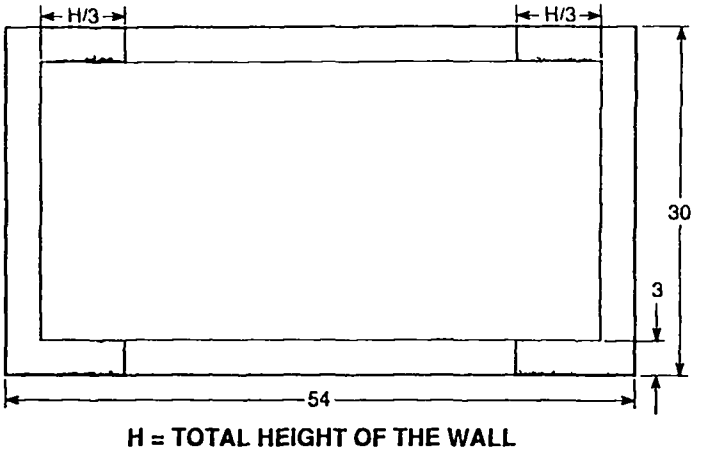

Fig. 73. ASCE method for assessing boundary element contribution to shear wall bending stiffness applied to CERL-1.

DISTRIBUTION

	Copies
Nuclear Regulatory Commission, RD, Laurel, Maryland	248
Technical Information Center, Oak Ridge, Tennessee	2
Los Alamos National Laboratory, Los Alamos, New Mexico	50
	300

NRC FORM 335 (2 84) NRCM 1102, 3201, 3202

U.S. NUCLEAR REGULATORY COMMISSION

BIBLIOGRAPHIC DATA SHEET

SEE INSTRUCTIONS ON THE REVERSE

1 REPORT NUMBER (Assigned by TIDC and Vol No., if any)

NUREG/CR-5237
LA-11444-MS

2 TITLE AND SUBTITLE

Use of Linear Reduced-Stiffness Analytical Models to Predict Seismic Response of Damaged Concrete Structures.

3 LEAVE BLANK

4 DATE REPORT COMPLETED

MONTH: September YEAR: 1988

5 AUTHOR(S)

C. R. Farrar, C. M. Alvord

6 DATE REPORT ISSUED

MONTH: May YEAR: 1989

7 PERFORMING ORGANIZATION NAME AND MAILING ADDRESS (Include Zip Code)

Los Alamos National Laboratory
P. O. Box 1663
Los Alamos, NM 87545

8 PROJECT/TASK/WORK UNIT NUMBER

9 FIN OR GRANT NUMBER

A7221

10 SPONSORING ORGANIZATION NAME AND MAILING ADDRESS (Include Zip Code)

Division of Engineering
Office of Nuclear Regulatory Research
U.S. Nuclear Regulatory Commission
Washington, DC 20555

11a TYPE OF REPORT

Technical

b PERIOD COVERED (Inclusive dates)

12 SUPPLEMENTARY NOTES

13 ABSTRACT (200 words or less)

An extensive analysis of previously measured seismic response data from the Seismic Category I Structures program was made to determine if reduced stiffness linear models can be used to predict the response of damaged nuclear power plant structures. Four structures ranging from one to three stories were analyzed for three different peak acceleration inputs. All inputs were scaled versions of the 1940 El Centro earthquake measured at the base of the test structures during shake-table testing. Comparisons between measured and analytically predicted responses were made in terms of floor response spectra. Stiffness in the analytical models was adjusted to obtain a match in frequency and damping was adjusted to obtain a match in amplitude. Results showed that the reduced-stiffness linear models could accurately predict the response of the damaged structures and these results were consistent with the response observed during static cyclic testing of similar structures. Changes in damping with excitation levels are also discussed. In addition to the analysis of the seismic response data, the stiffness of these structures was analyzed by a variety of methods currently used by industry and the stiffness values were compared with the values in the analytical models that best fit the measured response.

14 DOCUMENT ANALYSIS - a KEYWORDS/DESCRIPTORS

Seismology
Analytical Model

b IDENTIFIERS/OPEN ENDED TERMS

15 AVAILABILITY STATEMENT

Unlimited

16 SECURITY CLASSIFICATION

(This page) Unclassified

(This report) Unclassified

17 NUMBER OF PAGES

18 PRICE